Intracellular replication of *Pseudomonas aeruginosa* in epithelial cells requires suppression of the caspase-4 inflammasome

Abby R Kroken[1,2]*, Keith A Klein[1], Patrick S Mitchell[3], Vincent Nieto[2], Eric J Jedel[2], David J Evans[2,4], Suzanne M J Fleiszig[2, 5]

1. Department of Microbiology and Immunology, Loyola University Chicago, Maywood, IL USA
2. Herbert Wertheim School of Optometry & Vision Science, University of California, Berkeley, CA USA
3. Department of Microbiology, University of Washington, Seattle, WA, USA
4. College of Pharmacy, Touro University California, Vallejo, CA USA
5. Graduate Groups in Vision Sciences, Microbiology, and Infectious Diseases & Immunity, University of California, Berkeley, CA USA

* Corresponding author. Department of Microbiology and Immunology, Loyola University Chicago, Maywood, IL, USA. Email: akroken@luc.edu

Abstract

Pathogenesis of *Pseudomonas aeruginosa* infections can include bacterial survival inside epithelial cells. Previously, we showed this involves multiple roles played by the type three-secretion system (T3SS), and specifically the effector ExoS. This includes ExoS-dependent inhibition of a lytic host cell response that subsequently enables intracellular replication. Here, we studied the underlying cell death response to intracellular *P. aeruginosa*, comparing wild-type to T3SS mutants varying in capacity to induce cell death and that localize to different intracellular compartments. Results showed that corneal epithelial cell death induced by intracellular *P. aeruginosa* lacking the T3SS, which remains in vacuoles, correlated with activation of NF-κB as measured by p65 relocalization and TNFα transcription and secretion. Deletion of caspase-4 through CRISPR-Cas9 mutagenesis delayed cell death caused by these intracellular T3SS mutants. Caspase-4 deletion also countered more rapid cell death caused by T3SS effector-null mutants still expressing the TSSS apparatus that traffic to the host cell cytoplasm, and in doing so rescued intracellular replication normally dependent on ExoS. While HeLa cells lacked a lytic death response to T3SS mutants, it was found to be enabled by interferon gamma treatment. Together, these results show that epithelial cells can activate the noncanonical inflammasome pathway to limit proliferation of intracellular *P. aeruginosa*, not fully dependent on bacterially-driven vacuole escape. Since ExoS inhibits the lytic response, the data implicate targeting of caspase-4, an intracellular pattern recognition receptor, as another contributor to the role of ExoS in the intracellular lifestyle of *P. aeruginosa*.

39 **Importance**

40

41 *Pseudomonas aeruginosa* can exhibit an intracellular lifestyle within epithelial cells in vivo and in
42 vitro. The type three secretion system (T3SS) effector ExoS contributes via multiple mechanisms,
43 including extending the life of invaded host cells. Here, we aimed to understand the underlying
44 cell death inhibited by ExoS when *P. aeruginosa* is intracellular. Results showed that intracellular
45 *P. aeruginosa* lacking T3SS effectors could elicit rapid cell lysis via the non-canonical
46 inflammasome pathway. Caspase-4 contributed to cell lysis even when the intracellular bacteria
47 lacked the entire T33S and were consequently unable to escape vacuoles, representing a naturally
48 occurring subpopulation during wildtype infection. Together, the data show the caspase-4
49 inflammasome as an epithelial cell defense against intracellular *P. aeruginosa*, and implicate its
50 targeting as another mechanism by which ExoS preserves the host cell replicative niche.

51 **Introduction**

52

53 *Pseudomonas aeruginosa* is an opportunistic pathogen able to cause life- and vision-threatening
54 infections. While often referred to as an extracellular pathogen, *P. aeruginosa* can adopt an
55 intracellular lifestyle in various epithelial cell types, including corneal (1), bronchial (2), HeLa
56 cells (3) and in vivo (4). The ability of *P. aeruginosa* to replicate inside a host cell depends on the
57 type three secretion system (T3SS), with multiple roles played by the T3SS effector ExoS (5-7)
58 encoded by only invasive strains (8). ExoS is a bifunctional protein with both RhoGAP and ADP
59 ribosyltransferase (ADPr) activity. Broad substrate specificity of its ADPr domain (9, 10) enables
60 ExoS to impact multiple host processes (11, 12). Demonstrated effects of ExoS include
61 inactivation of host cell proliferative/survival signaling, disassembling the host cell cytoskeleton,
62 freezing of intracellular membrane trafficking, and disruption of ROS generation (9, 13-16). While
63 the molecular components of host cells targeted by ExoS to enable *P. aeruginosa* to replicate
64 intracellularly have not yet been elucidated, its ADPr activity is required, and mechanisms shown
65 include inhibition of autophagy (17) and evasion of lysosomes (18). Recently, we reported another
66 role for the ADPr activity of ExoS in intracellular persistence: preservation of host cell viability
67 (19), which was further explored here.

68

69 Eukaryotic host cells can sense and respond to intracellular pathogens (20, 21). Responses can
70 include initiation of regulated cell death pathways (22), which may subsequently be suppressed by
71 the bacteria to preserve their intracellular niche (23). One type of host response is pyroptosis, a
72 form of inflammatory lytic cell death (20). Multiple pyroptotic pathways have been identified,
73 each sensing different pathogen-associated molecular patterns (PAMPs) (24-27) or pathogen-

associated aberrant activities (28, 29). The sensor converges on the activation of a cysteine-aspartic protease: caspase-1 for canonical inflammasome pathways (30, 31), and caspase-4/5 for later-discovered pathways designated noncanonical (32-34). Inflammatory caspases cleave and activate gasdermin D (35, 36), which assembles into pores in host plasma membranes (37). This leads to release of cytokines IL-18 and IL-1β (38), and total lysis for many cell types (39).

P. aeruginosa effectors ExoS and ExoT can reduce IL-1β secretion in macrophages (40-42), suggesting an ability to interfere with inflammasome activation. Responses of macrophages and epithelial cells can differ. While inflammasomes are well-studied in macrophages and other myeloid cells, the repertoire of inflammasomes in epithelial cells is usually limited, and their functions less-well studied (43). One inflammasome pathway studied in some corneal diseases is NLRP3 (44, 45), which can detect numerous stimuli (46) including ionic flux from pore formation (47), lysosomal damaging agents (48), and bacterial RNA (49). However, not all relevant studies verified which corneal cell type expressed NLRP3, or explicitly determined if NLRP3 was activated, versus other inflammasome pathways that could also yield mature IL-1β. Recently, both caspase-4, which detects cytoplasmic LPS (50), and NLRP1, which detects pathogenic enzymatic activities and dsRNA (28, 51), were shown to be expressed and functional in the human corneal epithelium (52, 53). The Protein Atlas RNAseq data set for the corneal epithelial cell line hTCEpi (54) provides evidence for expression of caspase-4, caspase-5 (an additional LPS sensor (33, 55)), NLRP1, and NLRC4 (although its required sensor protein NAIP (56) was not detected) (57). While NLRP3, Pyrin, and AIM2 inflammasomes were not detected in these cells, this does not preclude upregulation upon specific stimuli or in vivo (57).

97 Having shown that the T3SS effector ExoS inhibits rapid cell lysis induced by intracellular *P.*
98 *aeruginosa* in corneal epithelial cells (19), we investigated the mechanisms underlying host cell
99 death elicited and modulated by intracellular *P. aeruginosa*. In doing so, we also leveraged the
100 finding that *P. aeruginosa* mutants lacking the entire T3SS (Δ*exsA* mutants) remain toxic to
101 corneal epithelial cells (58), contrasting with HeLa and CHO cells (59, 60). Results showed that
102 caspase-4 is required for rapid corneal epithelial cell death in response to *P. aeruginosa* invasion,
103 and in this way limits accumulation of an intracellular population of bacteria. While caspase-4-
104 dependent death occurred even if bacteria lacked the ability to leave vacuoles/enter the cytoplasm,
105 the response was faster when they could. Moreover, the death response was enabled in otherwise
106 unresponsive HeLa cells after stimulation with IFN-γ, which has been shown to limit cytoplasmic
107 sub-populations of *Salmonella* in a manner dependent on caspase-4 and GBP proteins (61). Since
108 ExoS inhibits the cell death response to intracellular *P. aeruginosa*, these results implicate ExoS
109 targeting a caspase-4-dependent response as another contributor to its well-established role in
110 intracellular survival by *P. aeruginosa*.
111
112 **Results**
113
114 ***P. aeruginosa* lacking the T3SS kill corneal epithelial cells but not HeLa cells.**
115 Generally, it is thought that *P. aeruginosa* mutants missing the T3SS (i.e., Δ*exsA* mutants) do not
116 kill epithelial cells, as shown for HeLa and CHO cells (59, 60). However, our published work has
117 shown that Δ*exsA* mutants are able to kill corneal epithelial cells, with contributions made by the
118 intracellular population (58). Recognizing that differences between cell types could assist in
119 deciphering mechanisms, we compared corneal epithelial cells (hTCEpi) (54) to HeLa cells using

120 the same methods. Impact of wild type PAO1, Δ*exsA* mutants (lacking the entire T3SS), and
121 Δ*exoSTY* mutants (lacking all known T3SS effectors) were studied. After a 3-hour invasion period,
122 extracellular bacteria were eliminated using the non-cell permeable antibiotic amikacin (3). Cell
123 death rates were measured with a FIJI macro that counts propidium iodide-positive nuclei
124 (permeabilized cells) and Hoechst-labeled nuclei (total cells) and reports a ratio over a 20-hour
125 post-infection period (19). The results confirmed that the two cell types were differentially
126 susceptible. Death rates for corneal epithelial cells were statistically similar between wild type and
127 Δ*exsA* mutants (**Figure 1A-B**), whereas HeLa cells infected with Δ*exsA* mutants showed very little
128 cell death even 20-h post infection (**Figure 1C-D**). In both cell types, the Δ*exoSTY* mutant yielded
129 the most rapid cell death as noted previously (19). Thus, corneal epithelial cells have an intrinsic
130 response to T3SS-null bacteria that is absent in HeLa cells, which may underly cell death occurring
131 in response to T3SS-positive bacteria.
132
133 **Dynamics of cell death in bacterially-occupied cells indicates roles for both T3SS machinery**
134 **and T3SS effectors.**
135 Visual inspection of infected cells suggested that not all cells were occupied by bacteria, and that
136 some non-occupied cells also died. Recognizing that this could skew results in bulk analyses of
137 cell death rates, we performed additional experiments to analyze only bacterially-occupied cells.
138 To enable this, we employed methods that allowed simultaneous detection of viable intracellular
139 bacteria and host cell (19). Wild type (PAO1) was compared to mutants lacking the entire T3SS
140 (Δ*exsA* mutants), and Δ*exoSTY* mutants lacking only T3SS effectors, using quantitative time lapse
141 imaging over 20 h. Since Δ*exsA* mutants do not kill HeLa cells, this analysis was only done using
142 corneal epithelial cells.

143

144 A method of detecting intracellular bacteria is needed, as amikacin-killed bacteria adhere to the
145 dishes and cells, making intracellular bacteria impossible to distinguish if using constitutive
146 fluorophore expression. To detect Δ*exsA* mutants inside cells, we previously used an arabinose-
147 inducible green fluorescent protein (GFP) expression vector pBAD-GFP (58). This method
148 involves induction of GFP expression using arabinose induction only after bacteria have invaded
149 cells and extracellular populations are killed (using amikacin). To keep experimental methods
150 consistent across samples, we explored the feasibility of using the induction method to also study
151 wild type and the Δ*exoSTY* mutants. In prior studies, these strains were visualized using a reporter
152 for the T3SS (3), because T3SS effectors are needed for intracellular replication (5, 19).
153 Unfortunately, fewer bacterial cells exhibited cytoplasmic spread using the arabinose induction
154 method compared to the T3SS reporter method (**Supplemental Figure 1A**). Moreover, while the
155 host cell death rate was similar for wild type PAO1 using both methods, it trended lower for
156 Δ*exoSTY* mutants expressing arabinose-induced GFP (**Supplemental Figure 1B)**. This suggested
157 GFP induction impacts the T3SS or some other factor relevant to cytoplasmic entry or spread: a
158 critical step for intracellular infection by wild type and Δ*exoSTY* mutants, but not for Δ*exsA*
159 mutants (which remain in vacuoles (58)). Indeed, T3SS effector secretion was reduced *in vitro*
160 using EGTA stimulation in the presence of arabinose when bacteria were also transformed with
161 pBAD-GFP (**Supplemental Figure 1C**). Thus, the T3SS expression plasmid pJNE05 was used to
162 study intracellular wild type and Δ*exoSTY* mutants, reserving arabinose induction of GFP for the
163 Δ*exsA* mutant. A limitation of this approach is that a sub-population of intracellular wild type
164 bacteria can remain T3SS-negative (58) and would be undetected in this analysis. However, the
165 advantage of this approach is that T3SS-dependent outcomes for intracellular bacteria can be

166 spatially isolated and examined independently, and then compared to homogenous populations of
167 Δ*exsA* mutants missing the T3SS apparatus.
168
169 Representative images from a time-lapse experiment using Δ*exsA* mutants are shown in **Figure**
170 **2A**. As expected, Δ*exsA* mutants localized to vacuoles inside cells (58). Most bacteria-occupied
171 cells died before the end of the 20 h assay, as shown by propidium iodide labeling of the nucleus.
172 However, **Figure 2B** shows an invaded cell still alive at 20 hours (no propidium iodide labeling),
173 representing a minority of cells at this time point. Videos of these time lapse experiments are
174 available in **Supplemental Movie 1**, which includes cells visualized in **Figures 2B and 2C** at 20
175 hours post infection. As shown previously, both wild type PAO1 and Δ*exoSTY* mutant infected
176 cells (shown in **Figure 2D)** replicated in the host cell cytoplasm after bacterial escape from
177 vacuoles (19). In both cases, most invaded cells died by the end of the assay, the Δ*exoSTY* mutant
178 doing so even more rapidly, expected due to lack of ExoS which normally counters cell death (19).
179 Hours following host cell death, propidium iodide of intracellular bacterial bodies eventually
180 replaced GFP signal (**Figure 2C and Supplemental Movie 1)**.
181
182 A computational approach was used to measure when populations of invaded cells died (19), and
183 a super violin plot visualization script developed by Kenny and Schoen was used to show
184 independent replicates as stripes single plots (62). This analysis examined 2,710 total invaded cells
185 over 6 replicate experiments. Results confirmed that intracellular Δ*exsA* mutants killed their
186 occupied cells at a broad range of time points, and the mean value of invaded cell survival times
187 was unexpectedly similar to wild type PAO1 (**Figure 3E**). The analysis also confirmed that the
188 intracellular Δ*exoSTY* mutant infections caused cell lysis at a more rapid rate, significantly

189 different from both wild type PAO1 and Δ*exsA* mutants (19). Thus, while cell death can be driven
190 by vacuolar contained bacteria, it was more rapid if bacteria could access the cytoplasm while
191 lacking effectors.
192
193 **T3SS-null mutant bacteria engage NF-κB signaling in corneal epithelial cells**.
194 To explore molecular mechanisms involved in *P. aeruginosa*-driven cell death, a real time PCR
195 array with genes involved in regulated cell death pathways was used to study candidate host
196 responses. Results showed that TNFα and BCL2A1 were upregulated in excess of fifty-fold in
197 both cell lines: (**Figure 3**). In the corneal cells, wild type and both mutants upregulated these genes,
198 while in HeLa cells, only the PAO1Δ*exoSTY* mutant had that impact.
199
200 Since TNFα and BCL2A1 can be regulated by NF-κB, activation of NF-κB was measured by
201 observing translocation of p65 to the nucleus (**Figure 4A**). In corneal epithelial cells, infection
202 with each tested strain caused p65 translocation, correlating with positive target gene transcription.
203 In HeLa cells, only infection with Δ*exoSTY* mutants led to p65 translocation (**Figure 4B)**. The
204 result with wild type PAO1 infection was difficult to discern due to cell rounding and low
205 cytoplasmic area; however, p65 appeared excluded from the nuclear region of HeLa cells (**Figure**
206 **4B, inset)**. Quantification of p65-positive nuclei was accomplished with an ImageJ macro (see
207 methods) (**Figure 4C and D**). This finding correlated with the transcriptional data, and is
208 suggestive of a mechanism in which the T3SS effectors limit p65 translocation in HeLa cells, but
209 not corneal epithelial cells. Since TNFα is associated with both apoptotic and necrotic cell death,
210 TNFα secretion from infected cells was measured by ELISA. The results showed that while wild
211 type PAO1 stimulated TNFα secretion from corneal epithelial cells, higher levels were detected

212 after infection with the Δ*exoSTY* mutant, and the Δ*exsA* mutant causing an intermediate response
213 (**Figure 4E**). TNFα was unable to be detected from HeLa cells infected with any strain.
214
215 Having found TNFα secretion levels correlated with cell death rates, we next asked if there was a
216 direct causative relationship that might also explain why some cells without visible intracellular
217 bacteria could also be killed. Thus, media from naïve cells or Δ*exsA* mutant-infected cells was
218 replaced with filter-sterilized media from Δ*exoSTY* mutant-infected cells (high TNFα). The
219 outcome showed that this did not enhance host cell death rates (**Figure 4F**), suggesting cell death
220 is not driven by a secreted factor such as TNFα, and requires bacteria present.
221
222 **Caspase-4 is involved in cell death response to intracellular *P. aeruginosa*.**
223 The morphology of invaded cell death included membrane integrity loss, intact nucleus, and
224 transient blebbing, all suggestive of pyroptosis (**Figure 2**) (22). Since caspase-4 can restrict
225 numerous other Gram-negative bacteria (61, 63), and the pathogen *Shigella* inhibits the caspase-4
226 inflammasome by multiple mechanisms to survive (64-66), and corneal epithelial cells were shown
227 to express caspase-4 (53), we tested the hypothesis that caspase-4 was involved in driving cell
228 death in response to intracellular *P. aeruginosa*. We generated *CASP4* knockout corneal epithelial
229 cells, and loss of caspase-4 protein was confirmed by Western blot (**Supplemental Figure 2**).
230 Control cell lines with non-targeting guide RNA were also generated using an identical selection
231 strategy and grown up as monoclonal lines; each exhibited death rates consistent with wild type,
232 non-transduced hTCEpi cells (**Supplemental Figure 3**).
233

234 Invasion by wild type PAO1 yielded similar cell death timing in both *CASP4* knockout cells as
235 wild type corneal epithelial cells (**Figure 5A, B, C**). In contrast, Δ*exoSTY* mutant-invaded cells
236 experienced significantly increased survival times (**Figure 5A, B, D**), which allowed substantial
237 accumulation of intracellular bacteria. A smaller but significant increase of invaded cell survival
238 times were also observed with PAO1Δ*exsA* mutant-occupied *CASP4* knockout cells (**Figure 5E**).
239 Bacterial replication was measured using summed GFP area contained in live cell masked region
240 generated by the FIJI macro (19). Results indicate increased bacterial replication in *CASP4*
241 knockout cells, with the most substantial increase observed in cells invaded by Δ*exoSTY* mutants
242 (**Figure 5F-H**). These data implicated the non-canonical inflammasome as a dominant response
243 to cytoplasmic invasion of T3SS-positive *P. aeruginosa* independently of the T3SS effectors,
244 and also show involvement in responding to vacuole-occupying bacteria. Unchanged cell death
245 timing for wild-type PAO1 in *CASP4* knockout cells aligns with our previously published data
246 showing that the T3SS effector exotoxins, specifically the ADP ribosyltransferase activity of
247 ExoS (19), counters cell death. Of note, while *CASP4* knockout reduced corneal epithelial cell
248 death associated with intracellular Δ*exsA* mutants, many of the cells still died by the end of the
249 20-hour imaging time frame (**Figure 1 and 5E**). This implies additional mechanisms for
250 recognizing vacuolar/T3SS-negative *P. aeruginosa* in addition to caspase-4 which are also
251 absent from HeLa cells.
252
253 Prior studies implicate Exotoxin S in delaying host cell lysis in response to invasion (19), thus
254 we examined the Δ*exoS* mutant in both wt corneal epithelial cells and *CASP4* knockout cells to
255 evaluate whether there is a role for ExoT and ExoY in suppressing caspase-4-mediated lysis or
256 supporting cytoplasmic bacterial grown (**Supplemental Figure 4**). Comparing to the

257 aforementioned study which tested strains encoding a single effector (e.g., Δ*exoST* or Δ*exoSY*)
258 (19), the ΔexoS mutant showed a similar phenotype to Δ*exoSY* mutant, which expresses only
259 ExoT: bacteria were unable to replicate substantially within in wt corneal epithelial cells
260 (**Supplemental Figure 4**). Bacterial mutant replication was rescued in *CASP4* knockout cells.
261 However, the timing of Δ*exoS*-invaded wt cell survival was irregular across the timeframe
262 observed (**Supplemental Figure 4C**), which may relate to ExoT's ability to block invasion (67,
263 68), or interfere with other inflammasomes (41). However, ExoT and ExoY were unable to
264 contribute to intracellular replication in cells with caspase-4.
265
266 **IFN-γ-stimulation enables HeLa cells to respond to intracellular *P. aeruginosa*.** HeLa cells
267 support cytoplasmic hyper-replication of *P. aeruginosa* before significant impact on host cell
268 viability occurs (3, 19). The bacterium *Salmonella* accomplishes a similar feat (69). Santos and
269 colleagues demonstrated that IFN-γ stimulation causes HeLa cells to lyse in response to
270 *Salmonella* entry into the cytosol, which was associated with upregulation of GBP proteins and
271 stimulation of the caspase-4 inflammasome. (61). We examined the impact of IFN-γ stimulation
272 on HeLa cells containing intracellular *P. aeruginosa* (**Figure 6**). The kinetics of wild type PAO1-
273 induced host cell death remained unchanged. However, the rate of cell death increased for both
274 PAO1Δ*exoSTY* and for PAO1Δ*exsA* infections (**Figure 1 and 6**) (59). IFN-γ-treated HeLa cells
275 occupied by Δ*exsA* mutants died over varied timepoints during the 20 hours of infection similar to
276 results for corneal epithelial cells. Aligning with the quick timing of cell lysis, PAO1Δ*exoSTY*
277 mutants were no longer able to replicate effectively in the cytoplasm of IFN-γ-treated HeLa cells.
278 Thus, IFN-γ-treated HeLa cells resembled corneal epithelial cells in their response to intracellular
279 *P. aeruginosa*.

280

281 **Discussion**

282

283 Invasive (ExoS-expressing) strains of *P. aeruginosa* can thrive inside a wide range of host cells
284 (2, 3, 5). After invading an epithelial cell, ExoS plays multiple roles in supporting intracellular
285 survival and replication, including inhibition of host cell lysis (19). This study aimed to
286 understand the underlying host response inhibited by ExoS. Knowing *P. aeruginosa* diversifies
287 intracellularly into vacuolar and cytoplasmic populations, bacteria in both locations trigger cell
288 death, their locations are determined by T3SS expression state, and that host cell lysis can be
289 suppressed by ExoS, we used T3SS mutants to interrogate mechanisms. Results showed that cell
290 death in response to cytoplasmic *P. aeruginosa* lacking T3SS effectors involved caspase-4; its
291 deletion inhibiting rapid pyroptotic lysis. Deletion of caspase-4 also partially alleviated cell death
292 caused by bacteria lacking the T3SS that were restricted to vacuoles (Δ*exsA* mutants). We further
293 found that while HeLa cells lack this response to intracellular *P. aeruginosa*, it could be induced
294 by IFN-γ, a stimulator of numerous genes including factors that assist in activation of the
295 caspase-4 inflammasome (61). This suggests one difference between corneal epithelial cells and
296 HeLa cells may be among interferon stimulated genes (such as GBP1-4), or the ability of corneal
297 epithelial cells to promptly upregulate inflammatory genes in response to *P. aeruginosa* (**Figure**
298 **3**). Since ExoS inhibits cell death in response to cytoplasmic bacteria (19), these findings
299 implicate ExoS-mediated interference with the non-canonical inflammasome pathway. ExoS is
300 only capable of prolonging cell survival to the same level as Δ*exsA* mutant-invaded cell death,
301 suggesting its role is restricted to the host response to cytoplasmic bacteria.

302

303 Since *P. aeruginosa* is often assumed an extracellular pathogen, previous studies of host
304 epithelial cell death have been from the perspective of extracellular bacteria. In that regard, ExoS
305 alone has cytotoxic activities. HeLa cells can undergo apoptotic cell death based on both
306 caspase-3 (59) and caspase-8 activity (70), and activation of apoptosis through JNK1 and
307 cytochrome c release (71). This was confirmed using a mammalian expression system for
308 introducing ExoS in the absence of bacteria, which showed it was sufficient to induce HeLa cell
309 apoptosis even in the absence of bacterial interaction (72). Placing our findings into the context
310 of these earlier HeLa cell studies, we note differences in our experimental systems: while they
311 explored mechanisms for cell death caused by ExoS, we studied cell death triggered by live
312 intracellular bacteria lacking ExoS. Were intracellular bacteria present in these assays, HeLa
313 cells would not have responded to them without stimulation. Our experiments also provide an
314 analysis of only invaded cells excluding extracellular bacteria to focus on impact of intracellular
315 bacteria, and used corneal cells which naturally respond to bacterial pathogen-associated
316 molecular patterns. We then showed that IFN-γ-stimulated HeLa cells respond in the same
317 manner: ExoS inhibits rather than drives a host cell death response. In sum, while introducing
318 ExoS in isolation is a useful surrogate for *in vitro* experimentation to address specific questions,
319 other factors modify the impact of ExoS in other situations. Despite differences in experimental
320 models, it remains important to reconcile outcomes. The innate ability of ExoS to both drive and
321 inhibit cell death, involving different types of regulated cell death, and correlating with presence
322 or absence of internalized *P. aeruginosa,* is interesting and worth exploring. Indeed, it could aid
323 in determining mechanisms by which ExoS blocks pyroptosis, given crosstalk between
324 pyroptosis and apoptosis (73).
325

326 The specific mechanism by which the ADPr activity of ExoS interferes with caspase-4-mediated
327 cell lysis remains to be identified. Recently, *Shigella flexneri* was shown to block the non-
328 canonical inflammasome by multiple mechanisms: caspase-4 inactivation from ADP-
329 riboxanation by the effector OspC3 (64, 65), ubiquitylating gasdermin D (74), and GBP1 (75) to
330 target each for degradation. ExoS is unique among bacterial ADP ribosyltransferases for having
331 numerous host substrates, though currently none are known to interact with the caspase-4/11
332 pathway (76). Since there are many possibilities to investigate, comprehensive identification of
333 uncharacterized ExoS substrates and their potential involvement will require a separate study.
334 Considering that *CASP4* knockout does not fully prevent cell death triggered by vacuole-bound
335 T3SS mutants (**Figure 6**), it would also be worth exploring which additional cell death pathways
336 are involved.
337
338 In summary, the results of this study demonstrate a role for caspase-4 in limiting intracellular
339 colonization of *P. aeruginosa* in ocular surface cells, a phenomenon triggered by the presence of
340 intracellular bacteria but inhibited by the T3SS effector ExoS. Importantly, the data support the
341 notion that *P. aeruginosa* can function as both an intracellular and extracellular pathogen,
342 suggestive of a T3SS effector function devoted to inhibition of an *intracellular* pattern
343 recognition receptor, consistent with its unusual capacity to adapt to its environment, survive
344 hardship, and exist ubiquitously. Ultimately, development of effective strategies to prevent or
345 treat the devastating infections caused by *P. aeruginosa* will require a thorough appreciation of
346 these complexities.
347
348 **Methods**

349 **Bacterial strains and cell lines.** *P. aeruginosa* strain PAO1 and isogenic mutants of *exsA*, or
350 ExoS/ExoT/ExoY, or ExoS were used for all infection experiments (77). Plasmids used for
351 visualization were pJNE05 (78) and pBAD-GFP (58). Plasmid selection was achieved with 100
352 µg/ml gentamicin. Corneal epithelial cells (hTCEpi) (54) were maintained in KGM-2 media
353 (Lonza) lacking gentamicin. HeLa cells were maintained in phenol red-free DMEM (Gibco) with
354 10% FBS.
355
356 **CRISPR-Cas9 knockout cell line.** Lentiviral particles for transduction were generated from
357 293T cells transfected with psPAX2 (Didier Trono, Addgene plasmid # 12260) and pMD.2
358 (Didier Trono, Addgene plasmid # 12259), combined with either Cas9 expression vector plenti-
359 Cas9-blast (Feng Zhang, Addgene plasmid # 52962) (79) or a guide RNA vector plenti-LIC-Puro
360 which was adapted for ligation-independent cloning (gifted by Moritz Gaidt) (80). Guide RNA
361 sequences targeting caspase-4 (5'- CCACAGAAAAAAGCCACTTA - 3') or a non-targeting
362 control sequence (5'- GACGGAGGCTAAGCGTCGCA - 3') were cloned into plenti-LIC-Puro
363 using ligation independent cloning. After six hours, media on 293T cells was replaced with
364 KGM-2. Media was collected at 48 hours and passed through a 0.45 µm filter and added directly
365 to hTCEpi cells, which were then centrifuged at 1200g for 90 minutes at 37°C. Antibiotic
366 selection with blasticidin (50 µg/ml) or puromycin (10 µg/ml) was performed after two days. For
367 generation of monoclonal lines, single cells were seeded in 96-well plates. Isolated colonies were
368 identified and grown up over approximately 12 days before transfer into 6-well plates to avoid
369 differentiation induced by crowding. *CASP4* knockout candidates were screened by Western
370 blot: lysates from a 6-well plate were collected in 150 µl RIPA buffer, frozen and thawed, and
371 then clarified by centrifugation for 20 minutes at 4ºC. Samples were run on 10% stain free gels

372 (Bio-Rad) and total protein visualized as a loading control prior to transfer to 0.2 µm PVDF
373 membrane. Membrane was blocked with Bio-Rad EveryBlot block and probed with anti-caspase-
374 4 antibody (Santa Cruz, sc-56056, 1:1000). Blot was washed using TBST, and antibody detected
375 with goat-anti-rabbit HRP (Bio-Rad, 1706515, 1:5000).
376
377 **Infection experiments.** One day preceding experiments, hTCEpi cells were plated on No. 1.5
378 glass-bottom 24 well plates (MatTek) in KGM-2 at 75% confluence with 1.15mM calcium to
379 induce differentiation (54). HeLa cells were maintained in DMEM with 10% FBS and plated at
380 50% confluence on optical plastic 8-well chambered coverslips (ibidi). Where indicated, 50
381 ng/ml IFN-γ (Peprotech) was added at 16 hours prior to infections of HeLa cells and maintained
382 throughout the infection and imaging.
383
384 Bacterial suspensions were made in PBS from 16-hour lawns grown on TSA media at 37°C. The
385 absorbance at 540 nm was measured, and MOI of 10 was calculated using OD540 of 1 equal to 4
386 x 10^8 CFU per mL. Bacteria were directly to cell culture media and allowed to infect for 3 hours.
387 For live imaging, Hoechst (0.8 µg/ml) was added to the cells prior to infections and allowed to
388 label the cells during the 3-hour infection period. Media was replaced with media containing the
389 antibiotic amikacin (200 µg/ml) and propidium iodide (0.8 µg/ml). Where needed, a 1:10
390 dilution of 10% arabinose in media was added at 3.75 hours post infection.
391
392 **RT-PCR arrays.** Cells in 10cm dishes were infected with PAO1, PAO1Δ*exoSTY*, or
393 PAO1Δ*exsA* for 3 hours at an MOI of 10, and media was replaced for 1 hour with 200 µg/ml
394 amikacin. At 4 hours, cells were washed twice in PBS and collected in 1ml TriReagent (Sigma).

395 RNA was purified using Zymo Direct-zol RNA MiniPrep. cDNA synthesis was performed with
396 the RT2 first strand kit (Qiagen) using 0.5µg RNA. RT PCR was performed on a Roche
397 LightCycler 96 using the The RT² Profiler™ PCR Array Human Cell Death PathwayFinder
398 (PAHS-212Z, Qiagen)w, and analyzed in Qiagen's Data Center Analysis Portal.
399 (https://geneglobe.qiagen.com/us/analyze).
400
401 **Fixed immunostaining.** Cells were seeded on No. 1.5 glass coverslips and infected as described
402 above. At four hours post infection, cells were washed twice in PBS and fixed in 4%
403 paraformaldehyde in PBS for 10 m. Cells were washed twice in PBS, and neutralized with 150
404 mM glycine in PBS for 10 m. Cells were washed twice in PBS, and permeabilized/blocked (5%
405 FBS, 2.5% cold fish skin gelatin, 0.1% TritonX-100, 0.05% Tween-20 in PBS) for 1 h. Antibody
406 in solution (2.5% FBS, 1.25% cold fish skin gelatin, 0.1% TritonX-100, 0.05% Tween-20 in
407 PBS) was incubated overnight at 4°C. Cells were washed 4 times (5 minutes), and secondary
408 antibodies were added in antibody solution for 1 h. Cells were washed once, labeled with DAPI
409 for 5 minutes, and washed twice (5 minutes). Coverslips were mounted using ProLong Diamond.
410
411 **Microscopy.** Images for Figs 1 and 4A, B were captured on a Nikon Ti-E inverted microscope
412 equipped with a Lumencor Spectra X LED Light Engine illumination source. All other images
413 were captured on a Ti2-E inverted microscope with X-Cite XYLIS XT720S Broad Spectrum
414 LED Illumination System. Both systems used Nikon perfect focus, an Okolab stage-top
415 incubation chamber, a DS-Qi2 CMOS camera, and CFI Plan Apochromat Lambda D 40X air NA
416 0.95 objective. Time lapse fields were selected between hours 3 and 4 without observing

417 fluorescence channels. Eight fields per condition were imaged hourly from 4 to 20 hours post
418 infection.
419
420 **Image Analysis.** Time-lapse images were computationally analyzed using two custom macros
421 written for the FIJI package of Image J aspreviously described (19). The code for measuring
422 rates of cell death for the whole population, and set of macros for tracking the invasion state of
423 cells is available in a GitHub repository: https://github.com/Llamero/Nuclei_analysis-macro.
424 Subsequent Python scripts for exporting the analysis TIF file and processing are available in the
425 following GitHub repository: https://github.com/abbykroken/cell_survival_with_bacteria. An
426 Image J macro for measuring a ratio of p65 stain intensity within the nucleus and the periplasmic
427 region has been made available in the following GitHub repository:
428 https://github.com/abbykroken/Nucleus-to-cell-ratio.
429
430 **In vitro T3SS effector secretion.** Bacteria were grown for 5 hours in 5ml TSB supplemented
431 with 100mM MSG and 1% glycerol at 37ºC with shaking at 200 rpm. EGTA (2mM) was added
432 to induce T3 secretion. OD 540 nm readings were taken prior to supernatant protein
433 concentration and used to normalize volumes. Bacteria were centrifuged at 12000g to clarify 1ml
434 of supernatant. Proteins were concentrated using TCA precipitation: 250 µl of 100% cold TCA
435 was added to 1 ml supernatant for 30 minutes and centrifuged at 14000g for 5 minutes. The
436 pellet was washed with 1 ml cold acetone twice and suspended in 4x laemmli buffer normalized
437 to starting OD (max volume 50 µl). Proteins were visualized using 10% stain-free gels (Bio-
438 Rad).
439

440 **Statistics.** Statistical analyses were performed and data presented using Graph Pad Prism 9. Super
441 violin plots were prepared using scripts published by Kenny and Schoen (62) and output images
442 aligned on axes generated in Graph Pad Prism 9. Data were shown as a mean ± standard deviation
443 (SD) of 3-6 independent experiments unless otherwise indicated. Comparison of two groups was
444 performed by Student's t-test, three or more groups by One-way ANOVA with Tukey's post-hoc
445 analysis. Comparison between two groups for total cell death rates overtime was performed by
446 multiple column t-tests for each timepoint, and the two samples that were compared are specified
447 in the figure legends. In each instance, * $P < 0.05$, ** $P < 0.01$, *** $P < 0.005$ and **** $P < 0.001$.
448

449 **Acknowledgements**

450 Thanks to Arne Rietsch (Case Western Reserve University, OH) for providing *P. aeruginosa*
451 strains and mutants, Timothy L Yahr (University of Iowa, IA) for plasmid pJNE05, and Danielle
452 M Robertson (University of Texas Southwestern, TX) for hTCEpi cells. Thanks to Benjamin E
453 Smith (University of California, Berkeley, CA) for continued support of FIJI image analysis
454 macros. We also thank Russell E Vance (University of California, Berkeley, CA) for helpful
455 suggestions during the course of this project.
456

457 ARK, PSM, VN, DJE, and SMJF designed the experiments; ARK, KAK, PSM, and EJJ performed
458 the experiments; ARK, KAK, PSM, VN, DJE, SMJF analyzed and interpreted the data; ARK,
459 DJE, and SMJF wrote the manuscript; ARK, DJE, and SMJF supervised the study.
460

461 This work was supported by the National Institutes of Health R01EY011221 (SMJF),
462 R01EY034239 (ARK), F32 EY025969 (ARK), DP2 AI154432 (PSM), P30 DK089507 (PSM),

F32 EY029152 (VN), and the Mallinckrodt Foundation (PSM). The funding agencies had no role in the study design, data collection and interpretation, or decision to submit the work for publication.

466 **Figure 1. Host cell death rates from *P. aeruginosa* mutant infections**. **(A)** Corneal epithelial
467 cells (hTCEpi) were infected with indicated strain: wt PAO1, PAO1Δ*exoSTY*, or PAO1Δ*exsA* for
468 3 hours at an MOI equal to 10. Hoechst (blue) was added to label nuclei. Non-associated bacteria
469 were removed, and media with amikacin and propidium iodide (red) was added to kill extracellular
470 bacteria. Cells were imaged hourly from 4 to 20 hours post infection. Select fields from indicated
471 times are shown. Scale bar = 50 µm. **(B)** The percent of cells positive for propidium iodide at each
472 timepoint was determined by using a custom FIJI macro to segment all nuclei from the Hoechst
473 channel, and all nuclei of dead cells in the propidium iodide channel. Multiple column t-tests were
474 performed comparing wt PAO1 and PAO1Δ*exsA*, and SD error bars are displayed from three
475 replicates. **(C)** Experiment was performed identically as in panel A, but using HeLa cells. Scale
476 bar = 50 µm. **(D)** Analysis was performed as in panel B, using the data obtained in panel C.
477
478 **Figure 2. Intracellular Δ*exsA* mutants kill invaded cells at a similar rate to wt PAO1-invaded**
479 **cells. (A)** Bacteria were transformed with an arabinose-inducible GFP plasmid. Corneal epithelial
480 cells (hTCEpi) were infected at an MOI of 10 and extracellular bacteria eliminated at 3 hours post
481 infection using amikacin. A final concentration of 1% arabinose was used to induce GFP in
482 surviving intracellular bacteria beginning at 3.5 hours post infection. Time lapse imaging was
483 conducted hourly from 4 to 20 hours, and host cell nuclei detected with Hoechst and propidium
484 iodide to determine time of death. Scale bar = 50 µm. Insets 1-2 show the boxed cell at 6 or 11
485 hours post infection, respectively. **(B)** An example of a live invaded cell from 20 hours post
486 infection. **(C)** Example of a dead invaded cell from 20 hours post infection, where the PI channel
487 has been saturated such that PI-positive bacteria can be visualized. Scale bar = 50 µm. **(D)** The
488 T3SS-GFP reporter pJNE05 was used to visualize wt PAO1 and PAO1Δ*exoSTY* infections, as

489 described previously (19), to compare to PAO1Δ*exsA* infections. Scale bar = 50 µm. Time lapses
490 from panels A through D are available as **Supplemental Movie 2**. **(E)** A computational analysis
491 approach was used to segregate only invaded cells, and determine their survival time in hours.
492 PAO1 condition includes 881 cells over six replicates; PAO1Δ*exoSTY*, 967 cells; PAO1Δ*exsA*,
493 862 cells. The survival times of all invaded cells were combined a single super violin plot. Mean
494 survival times with SD error bars are displayed, and significance determined by One-way
495 ANOVA. *** $P < 0.005$.
496
497 **Figure 3. Transcriptional responses of infected host cells. (A)** Corneal epithelial cells (hTCEpi)
498 were infected with wt PAO1, PAO1Δ*exoSTY*, or PAO1Δ*exsA* for 3 hours at an MOI equal to 10.
499 Non-associated bacteria were removed, and media with amikacin was added for 1 additional hour.
500 At four hours, RNA was purified from infected cells, and RT PCR analysis performed using a
501 commercial array for genes associated with specific cell death pathways. **(B)** Experiment
502 performed identically to panel A, except using HeLa cells.
503
504 **Figure 4. NF-κB signaling and the role of secreted factors in cell death. (A)** Corneal epithelial
505 cells (hTCEpi) were infected with wt PAO1, PAO1Δ*exoSTY*, or PAO1Δ*exsA* for 3 hours at an
506 MOI equal to 10. Then media was replaced with amikacin-containing media. Cells were fixed at
507 4 hours post infection and p65 localization was determined using immunofluorescent staining.
508 Nuclei were labeled with DAPI. Scale bar = 50 µm. **(B)** Experiment performed identically to panel
509 A, using HeLa cells. **(C)** Quantification of p65-positive nuclei from corneal epithelial cells, and
510 (**D**) HeLa cells. PAO1-infected HeLa cells were not able to be accurately quantified (indicated
511 using "ND") by automated analysis due to the small and irregular cytoplasmic area. (**E**) Corneal

512 epithelial cells were infected as described in panel A. Supernatant of infected cells was collected
513 at 4 hours post infection and TNFα measured by ELISA. **(D)** Supernatants of corneal epithelial
514 cells infected with PAO1Δ*exoSTY*, PAO1Δ*exsA*, or uninfected were collected at 4 hours post
515 infection and sterilized with 0.22 µm filter, and used as the replacement media on uninfected cells
516 or PAO1Δ*exsA* infected cells at 3 hours post infection, combined with amikacin and propidium
517 iodide. Hoechst was used to label all nuclei. The cell death rates were measured by time lapse
518 imaging, error bars display SD from three replicates.
519
520 **Figure 5. Caspase-4 limits intracellular replication and persistence of T3SS mutant bacteria.**
521 (A) Corneal epithelial cells (hTCEpi) or (B) cells knocked out for caspase-4 were infected with wt
522 PAO1, PAO1Δ*exoSTY* (each visualized by T3SS-GFP reporter) or PAO1Δ*exsA* (pBAD-GFP
523 induced) at an MOI of 10. Nuclei were labeled with Hoechst and propidium iodide. Extracellular
524 bacteria were eliminated with amikacin at 3 hours post infection, and imaged hourly from 4 to 20
525 hours post infection. Images from 4-9 hours post infection are shown. Scale bar = 50 µm. Full-
526 field time lapses are available as **Supplemental Movie 3**. (**B-D**) (C-D) Cells from indicated
527 infections were analyzed with a computational approach to segregate only invaded cells and
528 measure survival times in hours. Six replicates were combined into a single super violin plot. Mean
529 survival times with SD error bars are displayed, and significance determined by Student's t-test.
530 (F-H) GFP area was summed within the boundaries of live cells using the same data set as panels
531 C-E, and normalized to PAO1 (wt) at 4 hours post infection.
532
533 **Figure 6. IFN-γ-stimulated HeLa cells are not permissive for PAO1Δ*exoSTY* intracellular**
534 **replication nor PAO1Δ*exsA* intracellular persistence.** (A) HeLa cells were treated with 50

535 ng/ml IFN-γ for 16 hours prior to infection with wt PAO1, PAO1Δ*exoSTY* (each using the T3SS-
536 GFP reporter) or PAO1Δ*exsA* (pBAD-GFP induced) at an MOI of 10. Nuclei were labeled with
537 Hoechst and propidium iodide. Extracellular bacteria were eliminated with amikacin at 3 hours
538 post infection, and imaged hourly from 4 to 20 hours post infection. Select time frames are shown
539 at either 10 or 15 hours post infection. Scale bar = 50 µm. Full-field time lapses are available as
540 **Supplemental Movie 4**. **(B)** The rate of cell death was determined using host cell nuclear stains.
541 All panels are from the same experiment with only indicated bacterial strain shown. Error bars
542 show SD from three replicates. Multiple column t-tests were performed comparing IFN-γ-treated
543 cells to untreated.
544
545 **Supplemental Figure 1. GFP expression from plasmid pBAD-GFP suppresses the T3SS.** (A)
546 wt PAO1 was transformed with the T3SS reporter plasmid pJNE05, or the GFP inducible plasmid
547 pBAD-GFP and imaged hourly in time lapse. Example fields are shown in which bacteria
548 expressing GFP under the T3SS reporter exhibit intracellular spread and replication, whereas those
549 with inducible GFP show only limited intracellular replication. (B) The cell death rates of wt PAO1
550 or PAO1Δ*exoSTY* expressing GFP by either plasmid were measured, showing a trend of reduced
551 cell killing rates for PAO1Δ*exoSTY* when GFP expression is induced. (C) wt PAO1 with indicated
552 plasmid was grown for 5 hours in LB media with EGTA to induce the T3SS, and arabinose to
553 induce GFP. Supernatant proteins were concentrated by TCA precipitation, and the bands
554 constituting ExoS and ExoT are indicated.
555
556 **Supplemental Figure 2. Confirmation of caspase-4 deletion.** Lysates from wt hTCEpi cells or
557 caspase-4 candidate knockout cells were collected in RIPA buffer and clarified. Total protein was

558 visualized using Bio-Rad stain free gels prior to transfer. Blot was probed with anti-caspase-4
559 antibody.
560
561 **Supplemental Figure 3. Control monoclonal cells for CRISPR-Cas9 mutagenesis.** A control
562 cell line was generated using non-targeting guide RNA, and monoclonal line generated. Cells were
563 infected with wt PAO1, PAO1Δ*exoSTY* (each using the T3SS-GFP reporter) or PAO1Δ*exsA*
564 (pBAD-GFP induced) at an MOI of 10. Nuclei were labeled with Hoechst and Propidium iodide.
565 Extracellular bacteria were eliminated with amikacin at 3 hours post infection, and imaged hourly
566 from 4 to 20 hours post infection. Images were analyzed with a computational approach to
567 segregate invaded cells and measure survival times in hours. Three replicates were combined into
568 a single super violin plot. Mean survival times with SD error bars are displayed.
569
570 **Supplemental Figure 4. Host cell survival time and intracellular replication of single exotoxin**
571 **deletion of ExoS.** (A) Corneal epithelial cells or cells lacking caspase-4 were infected with wt
572 PAO1, PAO1Δ*exoSTY*, or PAO1Δ*exoS* (each visualized by T3SS-GFP reporter) at an MOI of 10.
573 Nuclei were labeled with Hoechst and propidium iodide. Extracellular bacteria were eliminated
574 with amikacin at 3 hours post infection, and imaged hourly from 4 to 20 hours post infection.
575 Images from 4-10 hours are shown. Scale bar = 50 µm. (B) GFP area was summed within the
576 boundaries of live cells and normalized to PAO1 (wt) at 4 hours post infection. (C) Cells from
577 indicated infections were analyzed with a computational approach to segregate only invaded cells
578 and measure survival times in hours. Mean survival times with SD error bars are displayed, and
579 significance determined by Student's t-test.
580

581

582 **Supplemental Movie 1. Corneal epithelial cells invaded by *P. aeruginosa* and mutants.**
583 Corneal epithelial cells (hTCEpi) were infected with wt PAO1, PAO1Δ*exoSTY* (each expressing
584 GFP by T3SS reporter), or PAO1Δ*exsA* (inducible GFP) for 3 hours at an MOI equal to 10. Then
585 media was replaced with amikacin-containing media. Arabinose was added to PAO1Δ*exsA*
586 condition at 3.5 hours post infection. Imaging was conducted hourly from 4 to 20 hours.

587

588 **Supplemental Movie 2. *CASP4* knockout corneal epithelial cells invaded by *P. aeruginosa***
589 **and mutants.** Corneal epithelial cells (hTCEpi) or *CASP4* knockout cells were infected with wt
590 PAO1, PAO1Δ*exoSTY* (each expressing GFP by T3SS reporter), or PAO1Δ*exsA* (inducible GFP)
591 for 3 hours at an MOI equal to 10. Then media was replaced with amikacin-containing media.
592 Arabinose was added to PAO1Δ*exsA* condition at 3.5 hours post infection. Imaging was conducted
593 hourly from 4 to 20 hours.

594

595 **Supplemental Movie 3. IFN-γ-stimulated HeLa cells invaded by *P. aeruginosa* and mutants.**
596 HeLa cells were treated with 50 ng/ml IFN-γ for 16 hours prior to infection with wt PAO1,
597 PAO1Δ*exoSTY* (each using the T3SS-GFP reporter) or PAO1Δ*exsA* (pBAD-GFP induced) at an
598 MOI of 10. Nuclei were labeled with Hoechst and Propidium iodide. Extracellular bacteria were
599 eliminated with amikacin at 3 hours post infection, and imaged hourly from 4 to 20 hours post
600 infection. Arabinose was added to PAO1Δ*exsA* condition at 3.5 hours post infection. Imaging was
601 conducted hourly from 4 to 20 hours. IFN-γ was maintained during infection and imaging.

602 **References**
603

604 1. Angus AA, Lee AA, Augustin DK, Lee EJ, Evans DJ, Fleiszig SM. 2008. Pseudomonas
605 aeruginosa induces membrane blebs in epithelial cells, which are utilized as a niche for
606 intracellular replication and motility. Infect Immun 76:1992-2001.
607 2. Jolly AL, Takawira D, Oke OO, Whiteside SA, Chang SW, Wen ER, Quach K, Evans DJ,
608 Fleiszig SM. 2015. Pseudomonas aeruginosa-induced bleb-niche formation in epithelial cells is
609 independent of actinomyosin contraction and enhanced by loss of cystic fibrosis transmembrane-
610 conductance regulator osmoregulatory function. mBio 6:e02533.
611 3. Kroken AR, Chen CK, Evans DJ, Yahr TL, Fleiszig SMJ. 2018. The Impact of ExoS on
612 Pseudomonas aeruginosa Internalization by Epithelial Cells Is Independent of fleQ and Correlates
613 with Bistability of Type Three Secretion System Gene Expression. mBio 9.
614 4. Fleiszig SM, Zaidi TS, Fletcher EL, Preston MJ, Pier GB. 1994. Pseudomonas aeruginosa
615 invades corneal epithelial cells during experimental infection. Infect Immun 62:3485-93.
616 5. Angus AA, Evans DJ, Barbieri JT, Fleiszig SM. 2010. The ADP-ribosylation domain of
617 Pseudomonas aeruginosa ExoS is required for membrane bleb niche formation and bacterial
618 survival within epithelial cells. Infect Immun 78:4500-10.
619 6. Sana TG, Baumann C, Merdes A, Soscia C, Rattei T, Hachani A, Jones C, Bennett KL, Filloux A,
620 Superti-Furga G, Voulhoux R, Bleves S. 2015. Internalization of Pseudomonas aeruginosa Strain
621 PAO1 into Epithelial Cells Is Promoted by Interaction of a T6SS Effector with the Microtubule
622 Network. mBio 6:e00712.
623 7. Garai P, Berry L, Moussouni M, Bleves S, Blanc-Potard AB. 2019. Killing from the inside:
624 Intracellular role of T3SS in the fate of Pseudomonas aeruginosa within macrophages revealed by
625 mgtC and oprF mutants. PLoS Pathog 15:e1007812.
626 8. Fleiszig SM, Zaidi TS, Preston MJ, Grout M, Evans DJ, Pier GB. 1996. Relationship between
627 cytotoxicity and corneal epithelial cell invasion by clinical isolates of Pseudomonas aeruginosa.
628 Infect Immun 64:2288-94.
629 9. Coburn J, Dillon ST, Iglewski BH, Gill DM. 1989. Exoenzyme S of Pseudomonas aeruginosa
630 ADP-ribosylates the intermediate filament protein vimentin. Infect Immun 57:996-8.
631 10. Riese MJ, Goehring UM, Ehrmantraut ME, Moss J, Barbieri JT, Aktories K, Schmidt G. 2002.
632 Auto-ADP-ribosylation of Pseudomonas aeruginosa ExoS. J Biol Chem 277:12082-8.
633 11. Goehring UM, Schmidt G, Pederson KJ, Aktories K, Barbieri JT. 1999. The N-terminal domain
634 of Pseudomonas aeruginosa exoenzyme S is a GTPase-activating protein for Rho GTPases. J Biol
635 Chem 274:36369-72.
636 12. Iglewski BH, Sadoff J, Bjorn MJ, Maxwell ES. 1978. Pseudomonas aeruginosa exoenzyme S: an
637 adenosine diphosphate ribosyltransferase distinct from toxin A. Proc Natl Acad Sci U S A
638 75:3211-5.
639 13. McGuffie EM, Frank DW, Vincent TS, Olson JC. 1998. Modification of Ras in eukaryotic cells
640 by Pseudomonas aeruginosa exoenzyme S. Infect Immun 66:2607-13.
641 14. Simon NC, Barbieri JT. 2014. Exoenzyme S ADP-ribosylates Rab5 effector sites to uncouple
642 intracellular trafficking. Infect Immun 82:21-8.
643 15. Maresso AW, Deng Q, Pereckas MS, Wakim BT, Barbieri JT. 2007. Pseudomonas aeruginosa
644 ExoS ADP-ribosyltransferase inhibits ERM phosphorylation. Cell Microbiol 9:97-105.
645 16. Deng Q, Barbieri JT. 2008. Modulation of host cell endocytosis by the type III cytotoxin,
646 Pseudomonas ExoS. Traffic 9:1948-57.
647 17. Rao L, De La Rosa I, Xu Y, Sha Y, Bhattacharya A, Holtzman MJ, Gilbert BE, Eissa NT. 2021.
648 Pseudomonas aeruginosa survives in epithelia by ExoS-mediated inhibition of autophagy and
649 mTOR. EMBO Rep 22:e50613.
650 18. Heimer SR, Evans DJ, Stern ME, Barbieri JT, Yahr T, Fleiszig SM. 2013. Pseudomonas
651 aeruginosa utilizes the type III secreted toxin ExoS to avoid acidified compartments within
652 epithelial cells. PLoS One 8:e73111.

653 19. Kroken AR, Gajenthra Kumar N, Yahr TL, Smith BE, Nieto V, Horneman H, Evans DJ, Fleiszig
654 SMJ. 2022. Exotoxin S secreted by internalized Pseudomonas aeruginosa delays lytic host cell
655 death. PLoS Pathog 18:e1010306.
656 20. Jorgensen I, Miao EA. 2015. Pyroptotic cell death defends against intracellular pathogens.
657 Immunol Rev 265:130-42.
658 21. Ulland TK, Ferguson PJ, Sutterwala FS. 2015. Evasion of inflammasome activation by microbial
659 pathogens. J Clin Invest 125:469-77.
660 22. Galluzzi L, Vitale I, Aaronson SA, Abrams JM, Adam D, Agostinis P, Alnemri ES, Altucci L,
661 Amelio I, Andrews DW, Annicchiarico-Petruzzelli M, Antonov AV, Arama E, Baehrecke EH,
662 Barlev NA, Bazan NG, Bernassola F, Bertrand MJM, Bianchi K, Blagosklonny MV, Blomgren
663 K, Borner C, Boya P, Brenner C, Campanella M, Candi E, Carmona-Gutierrez D, Cecconi F,
664 Chan FK, Chandel NS, Cheng EH, Chipuk JE, Cidlowski JA, Ciechanover A, Cohen GM,
665 Conrad M, Cubillos-Ruiz JR, Czabotar PE, D'Angiolella V, Dawson TM, Dawson VL, De
666 Laurenzi V, De Maria R, Debatin KM, DeBerardinis RJ, Deshmukh M, Di Daniele N, Di Virgilio
667 F, Dixit VM, Dixon SJ, et al. 2018. Molecular mechanisms of cell death: recommendations of the
668 Nomenclature Committee on Cell Death 2018. Cell Death Differ 25:486-541.
669 23. Cunha LD, Zamboni DS. 2013. Subversion of inflammasome activation and pyroptosis by
670 pathogenic bacteria. Front Cell Infect Microbiol 3:76.
671 24. Rayamajhi M, Zak DE, Chavarria-Smith J, Vance RE, Miao EA. 2013. Cutting edge: Mouse
672 NAIP1 detects the type III secretion system needle protein. J Immunol 191:3986-9.
673 25. Unterholzner L, Keating SE, Baran M, Horan KA, Jensen SB, Sharma S, Sirois CM, Jin T, Latz
674 E, Xiao TS, Fitzgerald KA, Paludan SR, Bowie AG. 2010. IFI16 is an innate immune sensor for
675 intracellular DNA. Nat Immunol 11:997-1004.
676 26. Shi J, Zhao Y, Wang Y, Gao W, Ding J, Li P, Hu L, Shao F. 2014. Inflammatory caspases are
677 innate immune receptors for intracellular LPS. Nature 514:187-92.
678 27. Martinon F, Agostini L, Meylan E, Tschopp J. 2004. Identification of bacterial muramyl
679 dipeptide as activator of the NALP3/cryopyrin inflammasome. Curr Biol 14:1929-34.
680 28. Sandstrom A, Mitchell PS, Goers L, Mu EW, Lesser CF, Vance RE. 2019. Functional
681 degradation: A mechanism of NLRP1 inflammasome activation by diverse pathogen enzymes.
682 Science 364.
683 29. Xu H, Yang J, Gao W, Li L, Li P, Zhang L, Gong YN, Peng X, Xi JJ, Chen S, Wang F, Shao F.
684 2014. Innate immune sensing of bacterial modifications of Rho GTPases by the Pyrin
685 inflammasome. Nature 513:237-41.
686 30. Poyet JL, Srinivasula SM, Tnani M, Razmara M, Fernandes-Alnemri T, Alnemri ES. 2001.
687 Identification of Ipaf, a human caspase-1-activating protein related to Apaf-1. J Biol Chem
688 276:28309-13.
689 31. Martinon F, Burns K, Tschopp J. 2002. The inflammasome: a molecular platform triggering
690 activation of inflammatory caspases and processing of proIL-beta. Molecular Cell 10:417-426.
691 32. Kayagaki N, Warming S, Lamkanfi M, Vande Walle L, Louie S, Dong J, Newton K, Qu Y, Liu J,
692 Heldens S, Zhang J, Lee WP, Roose-Girma M, Dixit VM. 2011. Non-canonical inflammasome
693 activation targets caspase-11. Nature 479:117-21.
694 33. Vigano E, Diamond CE, Spreafico R, Balachander A, Sobota RM, Mortellaro A. 2015. Human
695 caspase-4 and caspase-5 regulate the one-step non-canonical inflammasome activation in
696 monocytes. Nat Commun 6:8761.
697 34. Downs KP, Nguyen H, Dorfleutner A, Stehlik C. 2020. An overview of the non-canonical
698 inflammasome. Mol Aspects Med 76:100924.
699 35. He WT, Wan H, Hu L, Chen P, Wang X, Huang Z, Yang ZH, Zhong CQ, Han J. 2015.
700 Gasdermin D is an executor of pyroptosis and required for interleukin-1beta secretion. Cell Res
701 25:1285-98.
702 36. Kayagaki N, Stowe IB, Lee BL, O'Rourke K, Anderson K, Warming S, Cuellar T, Haley B,
703 Roose-Girma M, Phung QT, Liu PS, Lill JR, Li H, Wu J, Kummerfeld S, Zhang J, Lee WP,

704 Snipas SJ, Salvesen GS, Morris LX, Fitzgerald L, Zhang Y, Bertram EM, Goodnow CC, Dixit
705 VM. 2015. Caspase-11 cleaves gasdermin D for non-canonical inflammasome signalling. Nature
706 526:666-71.
707 37. Ding J, Wang K, Liu W, She Y, Sun Q, Shi J, Sun H, Wang DC, Shao F. 2016. Pore-forming
708 activity and structural autoinhibition of the gasdermin family. Nature 535:111-6.
709 38. Karmakar M, Minns M, Greenberg EN, Diaz-Aponte J, Pestonjamasp K, Johnson JL, Rathkey
710 JK, Abbott DW, Wang K, Shao F, Catz SD, Dubyak GR, Pearlman E. 2020. N-GSDMD
711 trafficking to neutrophil organelles facilitates IL-1beta release independently of plasma
712 membrane pores and pyroptosis. Nat Commun 11:2212.
713 39. DiPeso L, Ji DX, Vance RE, Price JV. 2017. Cell death and cell lysis are separable events during
714 pyroptosis. Cell Death Discov 3:17070.
715 40. Galle M, Schotte P, Haegman M, Wullaert A, Yang HJ, Jin S, Beyaert R. 2008. The
716 Pseudomonas aeruginosa Type III secretion system plays a dual role in the regulation of caspase-
717 1 mediated IL-1beta maturation. J Cell Mol Med 12:1767-76.
718 41. Mohamed MF, Gupta K, Goldufsky JW, Roy R, Callaghan LT, Wetzel DM, Kuzel TM, Reiser J,
719 Shafikhani SH. 2022. CrkII/Abl phosphorylation cascade is critical for NLRC4 inflammasome
720 activity and is blocked by Pseudomonas aeruginosa ExoT. Nat Commun 13:1295.
721 42. Ince D, Sutterwala FS, Yahr TL. 2015. Secretion of Flagellar Proteins by the Pseudomonas
722 aeruginosa Type III Secretion-Injectisome System. J Bacteriol 197:2003-11.
723 43. Churchill MJ, Mitchell PS, Rauch I. 2022. Epithelial Pyroptosis in Host Defense. J Mol Biol
724 434:167278.
725 44. Lian H, Fang X, Li Q, Liu S, Wei Q, Hua X, Li W, Liao C, Yuan X. 2022. NLRP3
726 Inflammasome-Mediated Pyroptosis Pathway Contributes to the Pathogenesis of Candida
727 albicans Keratitis. Front Med (Lausanne) 9:845129.
728 45. Zheng Q, Tan Q, Ren Y, Reinach PS, Li L, Ge C, Qu J, Chen W. 2018. Hyperosmotic Stress-
729 Induced TRPM2 Channel Activation Stimulates NLRP3 Inflammasome Activity in Primary
730 Human Corneal Epithelial Cells. Invest Ophthalmol Vis Sci 59:3259-3268.
731 46. Kelley N, Jeltema D, Duan Y, He Y. 2019. The NLRP3 Inflammasome: An Overview of
732 Mechanisms of Activation and Regulation. Int J Mol Sci 20.
733 47. Mariathasan S, Weiss DS, Newton K, McBride J, O'Rourke K, Roose-Girma M, Lee WP,
734 Weinrauch Y, Monack DM, Dixit VM. 2006. Cryopyrin activates the inflammasome in response
735 to toxins and ATP. Nature 440:228-32.
736 48. Hornung V, Bauernfeind F, Halle A, Samstad EO, Kono H, Rock KL, Fitzgerald KA, Latz E.
737 2008. Silica crystals and aluminum salts activate the NALP3 inflammasome through phagosomal
738 destabilization. Nature Immunology 9:847-856.
739 49. Kanneganti TD, Ozoren N, Body-Malapel M, Amer A, Park JH, Franchi L, Whitfield J, Barchet
740 W, Colonna M, Vandenabeele P, Bertin J, Coyle A, Grant EP, Akira S, Nunez G. 2006. Bacterial
741 RNA and small antiviral compounds activate caspase-1 through cryopyrin/Nalp3. Nature
742 440:233-6.
743 50. Kayagaki N, Wong MT, Stowe IB, Ramani SR, Gonzalez LC, Akashi-Takamura S, Miyake K,
744 Zhang J, Lee WP, Muszynski A, Forsberg LS, Carlson RW, Dixit VM. 2013. Noncanonical
745 inflammasome activation by intracellular LPS independent of TLR4. Science 341:1246-9.
746 51. Bauernfried S, Scherr MJ, Pichlmair A, Duderstadt KE, Hornung V. 2021. Human NLRP1 is a
747 sensor for double-stranded RNA. Science 371.
748 52. Griswold AR, Huang HC, Bachovchin DA. 2022. The NLRP1 Inflammasome Induces Pyroptosis
749 in Human Corneal Epithelial Cells. Invest Ophthalmol Vis Sci 63:2.
750 53. Xu S, Liu X, Liu X, Shi Y, Jin X, Zhang N, Li X, Zhang H. 2021. Wedelolactone ameliorates
751 Pseudomonas aeruginosa-induced inflammation and corneal injury by suppressing caspase-
752 4/5/11/GSDMD-mediated non-canonical pyroptosis. Exp Eye Res 211:108750.

753 54. Robertson DM, Li L, Fisher S, Pearce VP, Shay JW, Wright WE, Cavanagh HD, Jester JV. 2005.
754 Characterization of growth and differentiation in a telomerase-immortalized human corneal
755 epithelial cell line. Invest Ophthalmol Vis Sci 46:470-8.
756 55. Bitto NJ, Baker PJ, Dowling JK, Wray-McCann G, De Paoli A, Tran LS, Leung PL, Stacey KJ,
757 Mansell A, Masters SL, Ferrero RL. 2018. Membrane vesicles from Pseudomonas aeruginosa
758 activate the noncanonical inflammasome through caspase-5 in human monocytes. Immunol Cell
759 Biol 96:1120-1130.
760 56. Reyes Ruiz VM, Ramirez J, Naseer N, Palacio NM, Siddarthan IJ, Yan BM, Boyer MA,
761 Pensinger DA, Sauer JD, Shin S. 2017. Broad detection of bacterial type III secretion system and
762 flagellin proteins by the human NAIP/NLRC4 inflammasome. Proc Natl Acad Sci U S A
763 114:13242-13247.
764 57. Thul PJ, Akesson L, Wiking M, Mahdessian D, Geladaki A, Ait Blal H, Alm T, Asplund A,
765 Bjork L, Breckels LM, Backstrom A, Danielsson F, Fagerberg L, Fall J, Gatto L, Gnann C, Hober
766 S, Hjelmare M, Johansson F, Lee S, Lindskog C, Mulder J, Mulvey CM, Nilsson P, Oksvold P,
767 Rockberg J, Schutten R, Schwenk JM, Sivertsson A, Sjostedt E, Skogs M, Stadler C, Sullivan
768 DP, Tegel H, Winsnes C, Zhang C, Zwahlen M, Mardinoglu A, Ponten F, von Feilitzen K, Lilley
769 KS, Uhlen M, Lundberg E. 2017. A subcellular map of the human proteome. Science 356.
770 58. Kumar NG, Nieto V, Kroken AR, Jedel E, Grosser MR, Hallsten ME, Mettrucio MME, Yahr TL,
771 Evans DJ, Fleiszig SMJ. 2022. Pseudomonas aeruginosa Can Diversify after Host Cell Invasion
772 to Establish Multiple Intracellular Niches. mBio 13:e0274222.
773 59. Kaufman MR, Jia J, Zeng L, Ha U, Chow M, Jin S. 2000. Pseudomonas aeruginosa mediated
774 apoptosis requires the ADP-ribosylating activity of exoS. Microbiology (Reading) 146 (Pt
775 10):2531-2541.
776 60. Vallis AJ, Finck-Barbancon V, Yahr TL, Frank DW. 1999. Biological effects of Pseudomonas
777 aeruginosa type III-secreted proteins on CHO cells. Infect Immun 67:2040-4.
778 61. Santos JC, Boucher D, Schneider LK, Demarco B, Dilucca M, Shkarina K, Heilig R, Chen KW,
779 Lim RYH, Broz P. 2020. Human GBP1 binds LPS to initiate assembly of a caspase-4 activating
780 platform on cytosolic bacteria. Nat Commun 11:3276.
781 62. Kenny M, Schoen I. 2021. Violin SuperPlots: visualizing replicate heterogeneity in large data
782 sets. Mol Biol Cell 32:1333-1334.
783 63. Zamyatina A, Heine H. 2020. Lipopolysaccharide Recognition in the Crossroads of TLR4 and
784 Caspase-4/11 Mediated Inflammatory Pathways. Front Immunol 11:585146.
785 64. Kobayashi T, Ogawa M, Sanada T, Mimuro H, Kim M, Ashida H, Akakura R, Yoshida M,
786 Kawalec M, Reichhart JM, Mizushima T, Sasakawa C. 2013. The Shigella OspC3 effector
787 inhibits caspase-4, antagonizes inflammatory cell death, and promotes epithelial infection. Cell
788 Host Microbe 13:570-583.
789 65. Li Z, Liu W, Fu J, Cheng S, Xu Y, Wang Z, Liu X, Shi X, Liu Y, Qi X, Liu X, Ding J, Shao F.
790 2021. Shigella evades pyroptosis by arginine ADP-riboxanation of caspase-11. Nature
791 doi:10.1038/s41586-021-04020-1.
792 66. Goers L, Kim K, Canning PJ, Stedman TC, Mou X, Ernst NH, Coers J, Lesser CF. 2022. *Shigella*
793 IpaH9.8 limits GBP1-dependent LPS release from intracytosolic bacteria to suppress caspase-4
794 activation. bioRxiv doi:10.1101/2022.11.14.516511:2022.11.14.516511.
795 67. Cowell BA, Chen DY, Frank DW, Vallis AJ, Fleiszig SM. 2000. ExoT of cytotoxic Pseudomonas
796 aeruginosa prevents uptake by corneal epithelial cells. Infect Immun 68:403-6.
797 68. Garrity-Ryan L, Kazmierczak B, Kowal R, Comolli J, Hauser A, Engel JN. 2000. The arginine
798 finger domain of ExoT contributes to actin cytoskeleton disruption and inhibition of
799 internalization of Pseudomonas aeruginosa by epithelial cells and macrophages. Infect Immun
800 68:7100-13.
801 69. Knodler LA, Nair V, Steele-Mortimer O. 2014. Quantitative assessment of cytosolic Salmonella
802 in epithelial cells. PLoS One 9:e84681.

803 70. Alaoui-El-Azher M, Jia J, Lian W, Jin S. 2006. ExoS of Pseudomonas aeruginosa induces
804 apoptosis through a Fas receptor/caspase 8-independent pathway in HeLa cells. Cell Microbiol
805 8:326-38.
806 71. Jia J, Alaoui-El-Azher M, Chow M, Chambers TC, Baker H, Jin S. 2003. c-Jun NH2-terminal
807 kinase-mediated signaling is essential for Pseudomonas aeruginosa ExoS-induced apoptosis.
808 Infect Immun 71:3361-70.
809 72. Jia J, Wang Y, Zhou L, Jin S. 2006. Expression of Pseudomonas aeruginosa toxin ExoS
810 effectively induces apoptosis in host cells. Infect Immun 74:6557-70.
811 73. Taabazuing CY, Okondo MC, Bachovchin DA. 2017. Pyroptosis and Apoptosis Pathways
812 Engage in Bidirectional Crosstalk in Monocytes and Macrophages. Cell Chem Biol 24:507-514
813 e4.
814 74. Luchetti G, Roncaioli JL, Chavez RA, Schubert AF, Kofoed EM, Reja R, Cheung TK, Liang Y,
815 Webster JD, Lehoux I, Skippington E, Reeder J, Haley B, Tan MW, Rose CM, Newton K,
816 Kayagaki N, Vance RE, Dixit VM. 2021. Shigella ubiquitin ligase IpaH7.8 targets gasdermin D
817 for degradation to prevent pyroptosis and enable infection. Cell Host Microbe
818 doi:10.1016/j.chom.2021.08.010.
819 75. Li P, Jiang W, Yu Q, Liu W, Zhou P, Li J, Xu J, Xu B, Wang F, Shao F. 2017. Ubiquitination and
820 degradation of GBPs by a Shigella effector to suppress host defence. Nature 551:378-383.
821 76. Barbieri JT, Sun J. 2004. Pseudomonas aeruginosa ExoS and ExoT. Rev Physiol Biochem
822 Pharmacol 152:79-92.
823 77. Sun Y, Karmakar M, Taylor PR, Rietsch A, Pearlman E. 2012. ExoS and ExoT ADP
824 ribosyltransferase activities mediate Pseudomonas aeruginosa keratitis by promoting neutrophil
825 apoptosis and bacterial survival. J Immunol 188:1884-95.
826 78. Urbanowski ML, Brutinel ED, Yahr TL. 2007. Translocation of ExsE into Chinese hamster ovary
827 cells is required for transcriptional induction of the Pseudomonas aeruginosa type III secretion
828 system. Infect Immun 75:4432-9.
829 79. Sanjana NE, Shalem O, Zhang F. 2014. Improved vectors and genome-wide libraries for CRISPR
830 screening. Nat Methods 11:783-784.
831 80. Schmidt T, Schmid-Burgk JL, Hornung V. 2015. Synthesis of an arrayed sgRNA library targeting
832 the human genome. Sci Rep 5:14987.
833
834

Figure 1

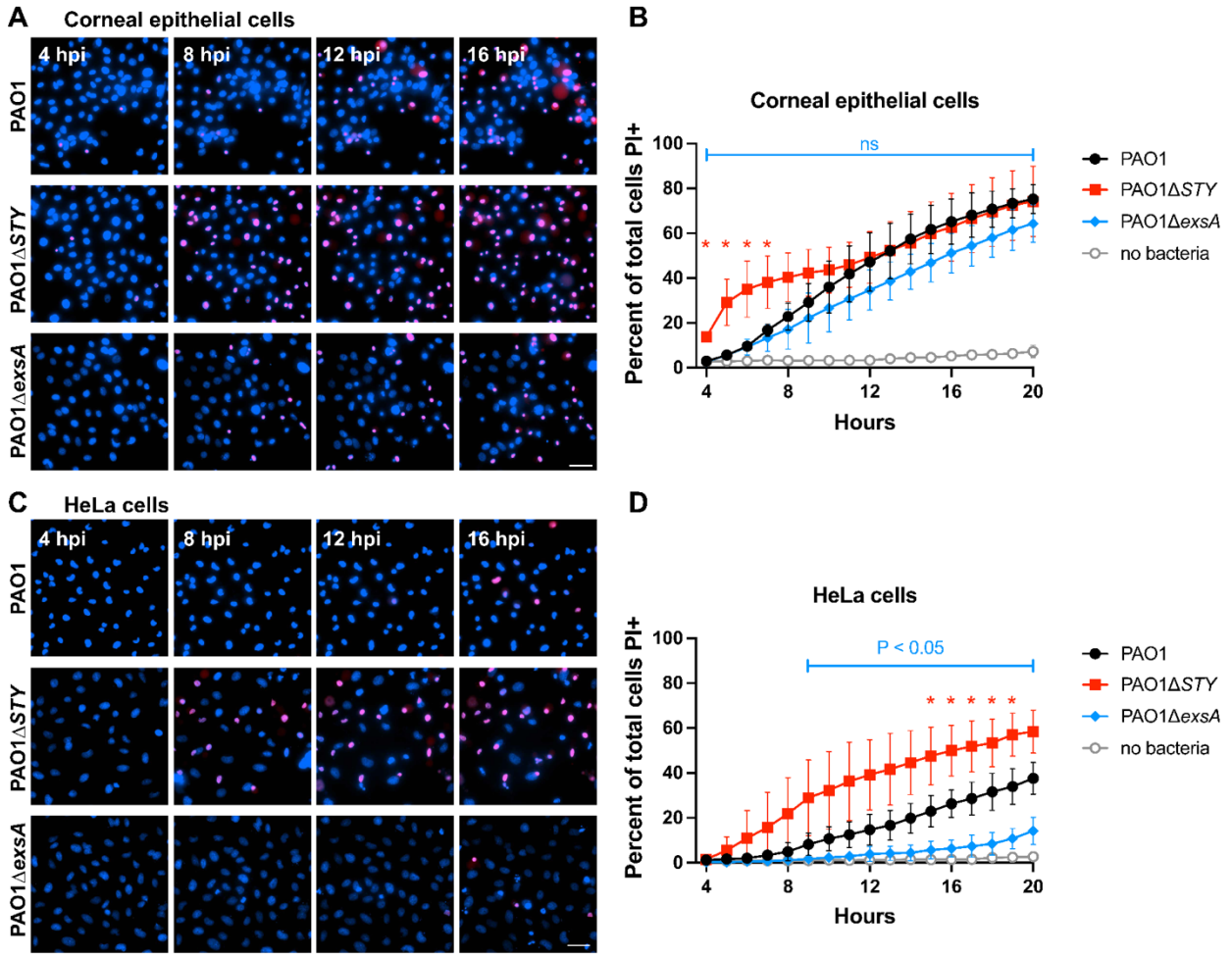

Figure 1. Host cell death rates from *P. aeruginosa* mutant infections. **(A)** Corneal epithelial cells (hTCEpi) were infected with indicated strain: wt PAO1, PAO1Δ*exoSTY*, or PAO1Δ*exsA* for 3 hours at an MOI equal to 10. Hoechst (blue) was added to label nuclei. Non-associated bacteria were removed, and media with amikacin and propidium iodide (red) was added to kill extracellular bacteria. Cells were imaged hourly from 4 to 20 hours post infection. Select fields from indicated times are shown. Scale bar = 50 µm. **(B)** The percent of cells positive for propidium iodide at each timepoint was determined by using a custom FIJI macro to segment all nuclei from the Hoechst channel, and all nuclei of dead cells in the propidium iodide channel. Multiple column t-tests were performed comparing wt PAO1 and PAO1Δ*exsA*, and SD error bars are displayed from three replicates. **(C)** Experiment was performed identically as in panel A, but using HeLa cells. Scale bar = 50 µm. **(D)** Analysis was performed as in panel B, using the data obtained in panel C.

Figure 2

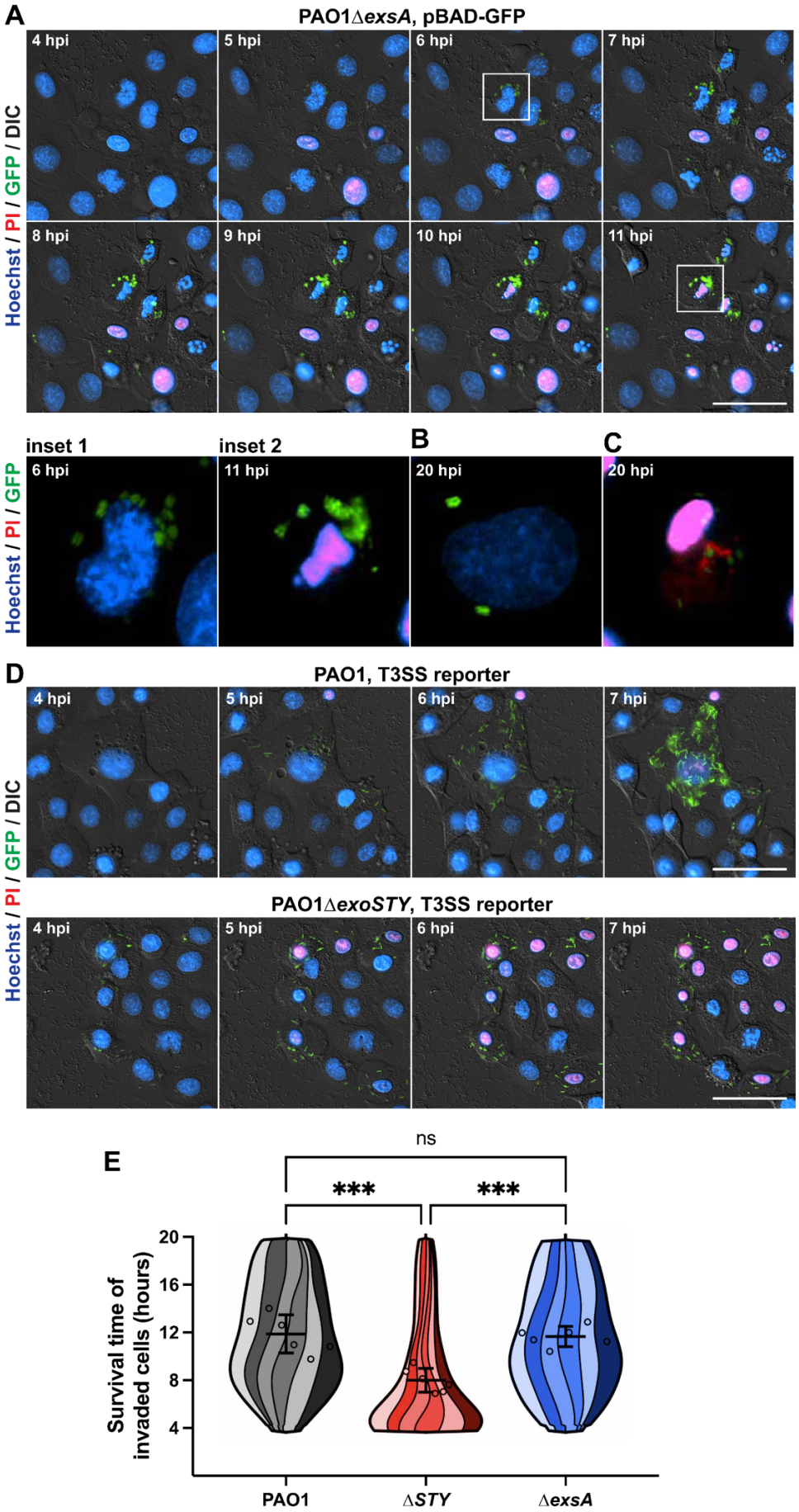
A
PAO1ΔexsA, pBAD-GFP
4 hpi
5 hpi
6 hpi
7 hpi
8 hpi
9 hpi
10 hpi
11 hpi
Hoechst / PI / GFP / DIC
inset 1
inset 2
B
C
6 hpi
11 hpi
20 hpi
20 hpi
Hoechst / PI / GFP
D
PAO1, T3SS reporter
4 hpi
5 hpi
6 hpi
7 hpi
PAO1ΔexoSTY, T3SS reporter
4 hpi
5 hpi
6 hpi
7 hpi
Hoechst / PI / GFP / DIC
E
ns
***
***
Survival time of invaded cells (hours)
20
16
12
8
4
PAO1
ΔSTY
ΔexsA

Figure 2. Intracellular Δ*exsA* mutants kill invaded cells at a similar rate to wt PAO1-invaded cells. (A) Bacteria were transformed with an arabinose-inducible GFP plasmid. Corneal epithelial cells (hTCEpi) were infected at an MOI of 10 and extracellular bacteria eliminated at 3 hours post infection using amikacin. A final concentration of 1% arabinose was used to induce GFP in surviving intracellular bacteria beginning at 3.5 hours post infection. Time lapse imaging was conducted hourly from 4 to 20 hours, and host cell nuclei detected with Hoechst and propidium iodide to determine time of death. Scale bar = 50 µm. Insets 1-2 show the boxed cell at 6 or 11 hours post infection, respectively. **(B)** An example of a live invaded cell from 20 hours post infection. **(C)** Example of a dead invaded cell from 20 hours post infection, where the PI channel has been saturated such that PI-positive bacteria can be visualized. Scale bar = 50 µm. **(D)** The T3SS-GFP reporter pJNE05 was used to visualize wt PAO1 and PAO1Δ*exoSTY* infections, as described previously (19), to compare to PAO1Δ*exsA* infections. Scale bar = 50 µm. Time lapses from panels A through D are available as **Supplemental Movie 2**. **(E)** A computational analysis approach was used to segregate only invaded cells, and determine their survival time in hours. PAO1 condition includes 881 cells over six replicates; PAO1Δ*exoSTY*, 967 cells; PAO1Δ*exsA*, 862 cells. The survival times of all invaded cells were combined a single super violin plot. Mean survival times with SD error bars are displayed, and significance determined by One-way ANOVA. *** $P < 0.005$.

Figure 3

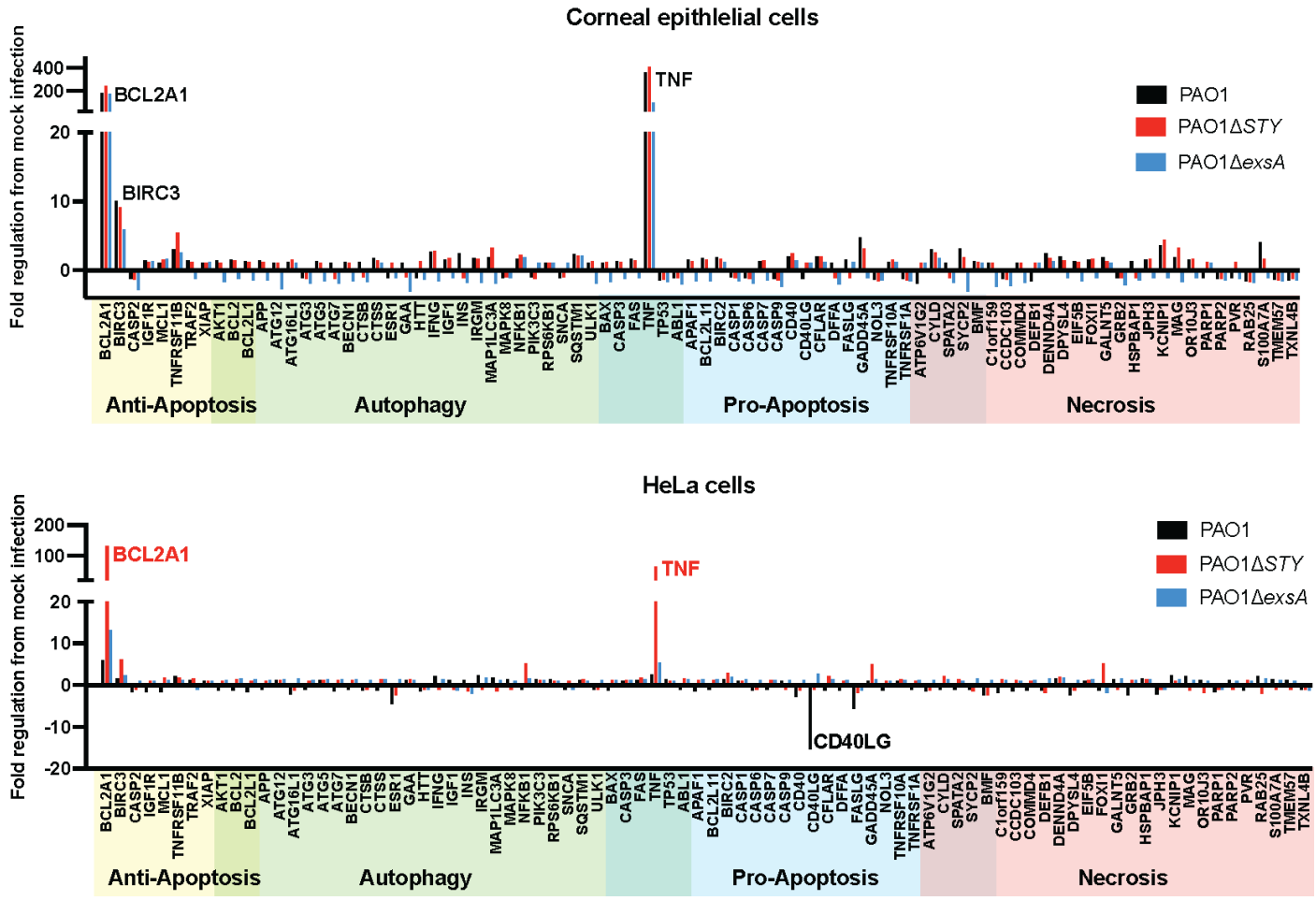

Figure 3. Transcriptional responses of infected host cells. (A) Corneal epithelial cells (hTCEpi) were infected with wt PAO1, PAO1Δ*exoSTY*, or PAO1Δ*exsA* for 3 hours at an MOI equal to 10. Non-associated bacteria were removed, and media with amikacin was added for 1 additional hour. At four hours, RNA was purified from infected cells, and RT PCR analysis performed using a commercial array for genes associated with specific cell death pathways. **(B)** Experiment performed identically to panel A, except using HeLa cells.

Figure 4.

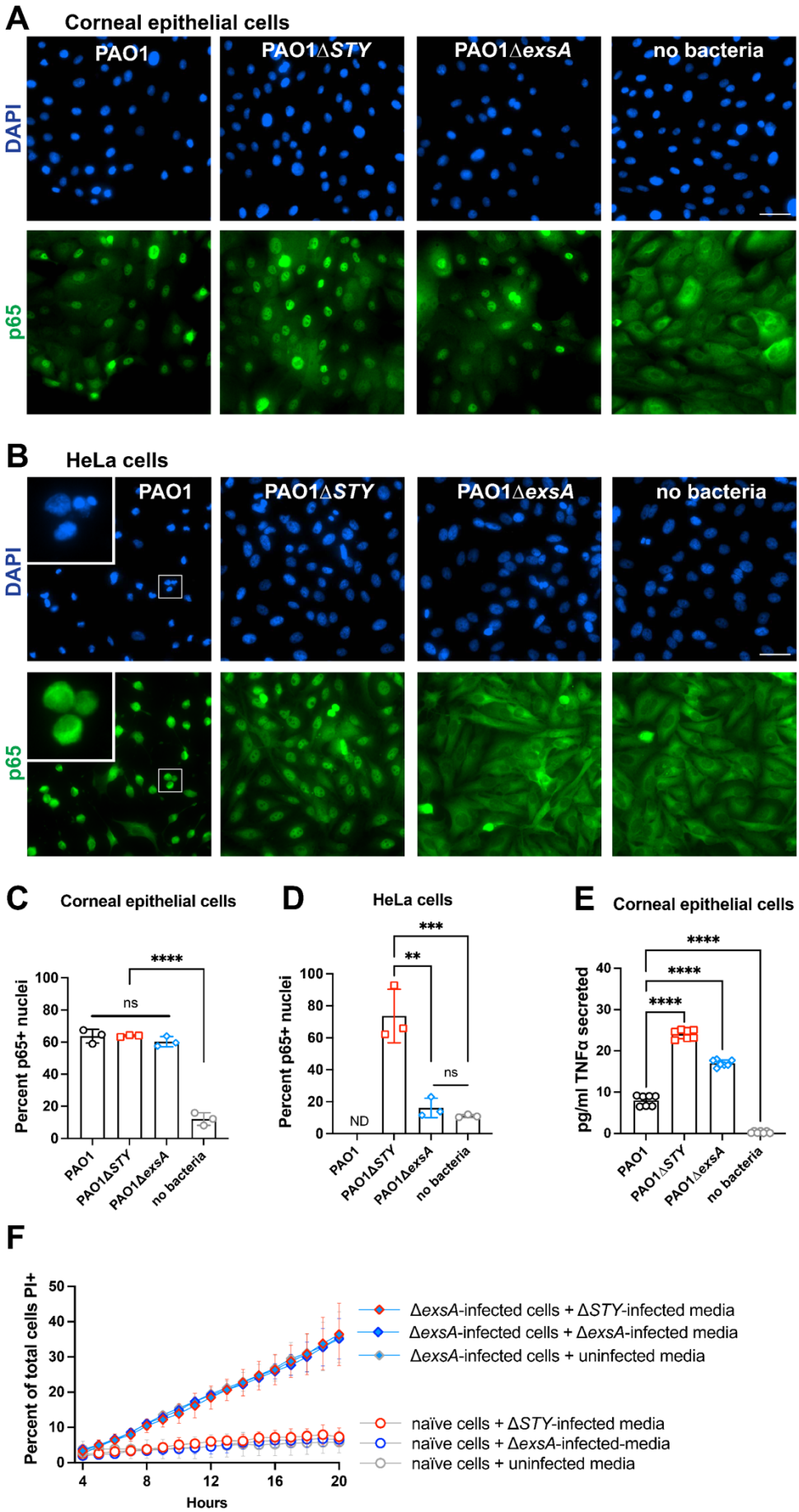
A
Corneal epithelial cells
PAO1
PAO1ΔSTY
PAO1ΔexsA
no bacteria
DAPI
p65
B
HeLa cells
PAO1
PAO1ΔSTY
PAO1ΔexsA
no bacteria
DAPI
p65
C
Corneal epithelial cells
Percent p65+ nuclei
****
ns
PAO1
PAO1ΔSTY
PAO1ΔexsA
no bacteria
D
HeLa cells
Percent p65+ nuclei
***
**
ns
ND
PAO1
PAO1ΔSTY
PAO1ΔexsA
no bacteria
E
Corneal epithelial cells
pg/ml TNFα secreted
****
****
****
PAO1
PAO1ΔSTY
PAO1ΔexsA
no bacteria
F
Percent of total cells PI+
Hours
ΔexsA-infected cells + ΔSTY-infected media
ΔexsA-infected cells + ΔexsA-infected media
ΔexsA-infected cells + uninfected media
naïve cells + ΔSTY-infected media
naïve cells + ΔexsA-infected-media
naïve cells + uninfected media

Figure 4. NF-κB signaling and the role of secreted factors in cell death. (A) Corneal epithelial cells (hTCEpi) were infected with wt PAO1, PAO1Δ*exoSTY*, or PAO1Δ*exsA* for 3 hours at an MOI equal to 10. Then media was replaced with amikacin-containing media. Cells were fixed at 4 hours post infection and p65 localization was determined using immunofluorescent staining. Nuclei were labeled with DAPI. Scale bar = 50 µm. **(B)** Experiment performed identically to panel A, using HeLa cells. **(C)** Quantification of p65-positive nuclei from corneal epithelial cells, and (**D**) HeLa cells. PAO1-infected HeLa cells were not able to be accurately quantified (indicated using "ND") by automated analysis due to the small and irregular cytoplasmic area. (**E**) Corneal epithelial cells were infected as described in panel A. Supernatant of infected cells was collected at 4 hours post infection and TNFα measured by ELISA. **(D)** Supernatants of corneal epithelial cells infected with PAO1Δ*exoSTY*, PAO1Δ*exsA*, or uninfected were collected at 4 hours post infection and sterilized with 0.22 µm filter, and used as the replacement media on uninfected cells or PAO1Δ*exsA* infected cells at 3 hours post infection, combined with amikacin and propidium iodide. Hoechst was used to label all nuclei. The cell death rates were measured by time lapse imaging, error bars display SD from three replicates.

Figure 5

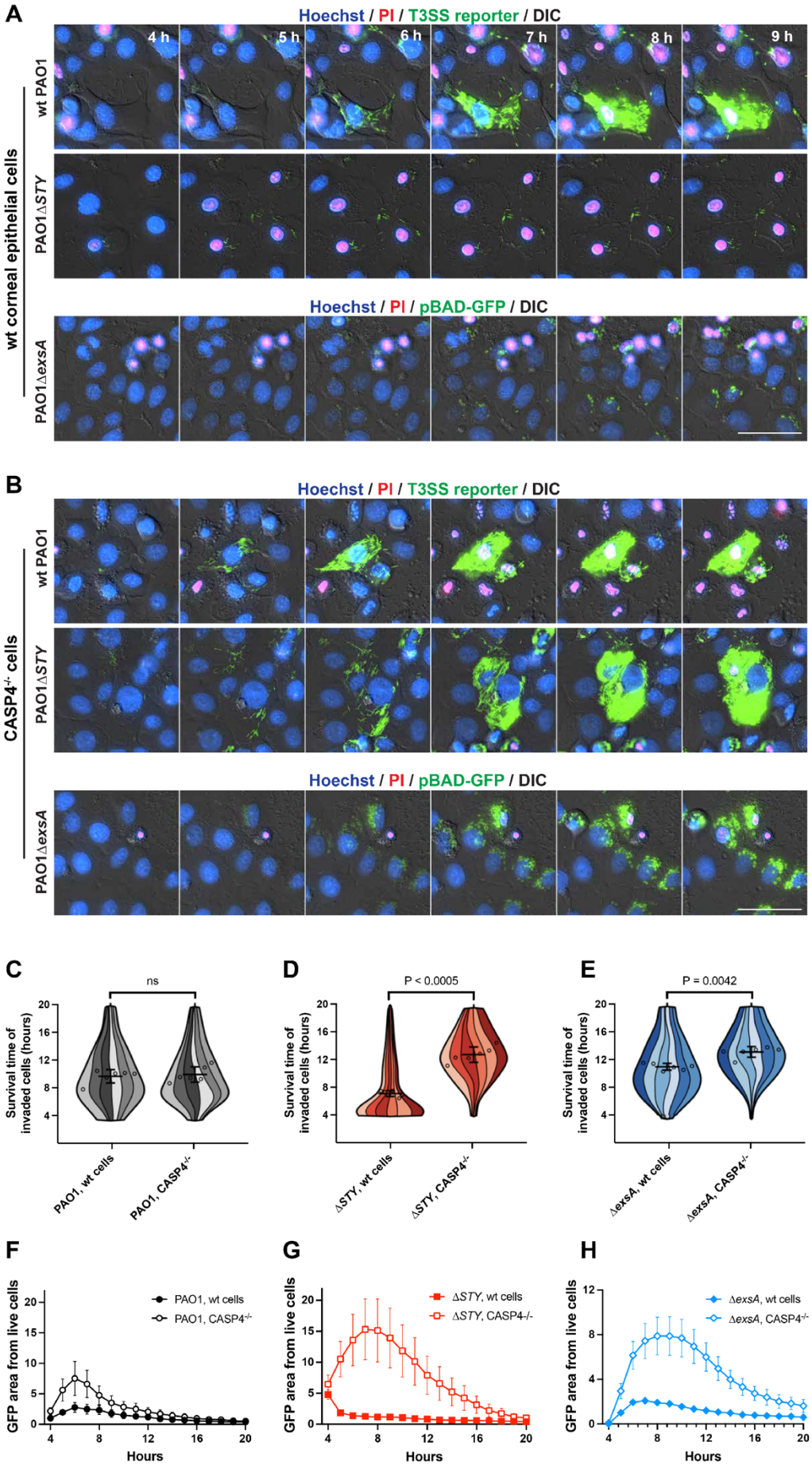
A
Hoechst / PI / T3SS reporter / DIC
4 h
5 h
6 h
7 h
8 h
9 h
wt corneal epithelial cells
wt PAO1
PAO1ΔSTY
Hoechst / PI / pBAD-GFP / DIC
PAO1ΔexsA
B
Hoechst / PI / T3SS reporter / DIC
CASP4-/- cells
wt PAO1
PAO1ΔSTY
Hoechst / PI / pBAD-GFP / DIC
PAO1ΔexsA
C
ns
Survival time of invaded cells (hours)
PAO1, wt cells
PAO1, CASP4-/-
D
P < 0.0005
ΔSTY, wt cells
ΔSTY, CASP4-/-
E
P = 0.0042
ΔexsA, wt cells
ΔexsA, CASP4-/-
F
GFP area from live cells
PAO1, wt cells
PAO1, CASP4-/-
Hours
G
ΔSTY, wt cells
ΔSTY, CASP4-/-
H
ΔexsA, wt cells
ΔexsA, CASP4-/-

Figure 5. Caspase-4 limits intracellular replication and persistence of T3SS mutant bacteria. (A) Corneal epithelial cells (hTCEpi) or (B) cells knocked out for caspase-4 were infected with wt PAO1, PAO1Δ*exoSTY* (each visualized by T3SS-GFP reporter) or PAO1Δ*exsA* (pBAD-GFP induced) at an MOI of 10. Nuclei were labeled with Hoechst and propidium iodide. Extracellular bacteria were eliminated with amikacin at 3 hours post infection, and imaged hourly from 4 to 20 hours post infection. Images from 4-9 hours post infection are shown. Scale bar = 50 µm. Full-field time lapses are available as **Supplemental Movie 3**. (**B-D**) (C-D) Cells from indicated infections were analyzed with a computational approach to segregate only invaded cells and measure survival times in hours. Six replicates were combined into a single super violin plot. Mean survival times with SD error bars are displayed, and significance determined by Student's t-test. (F-H) GFP area was summed within the boundaries of live cells using the same data set as panels C-E, and normalized to PAO1 (wt) at 4 hours post infection.

Figure 6

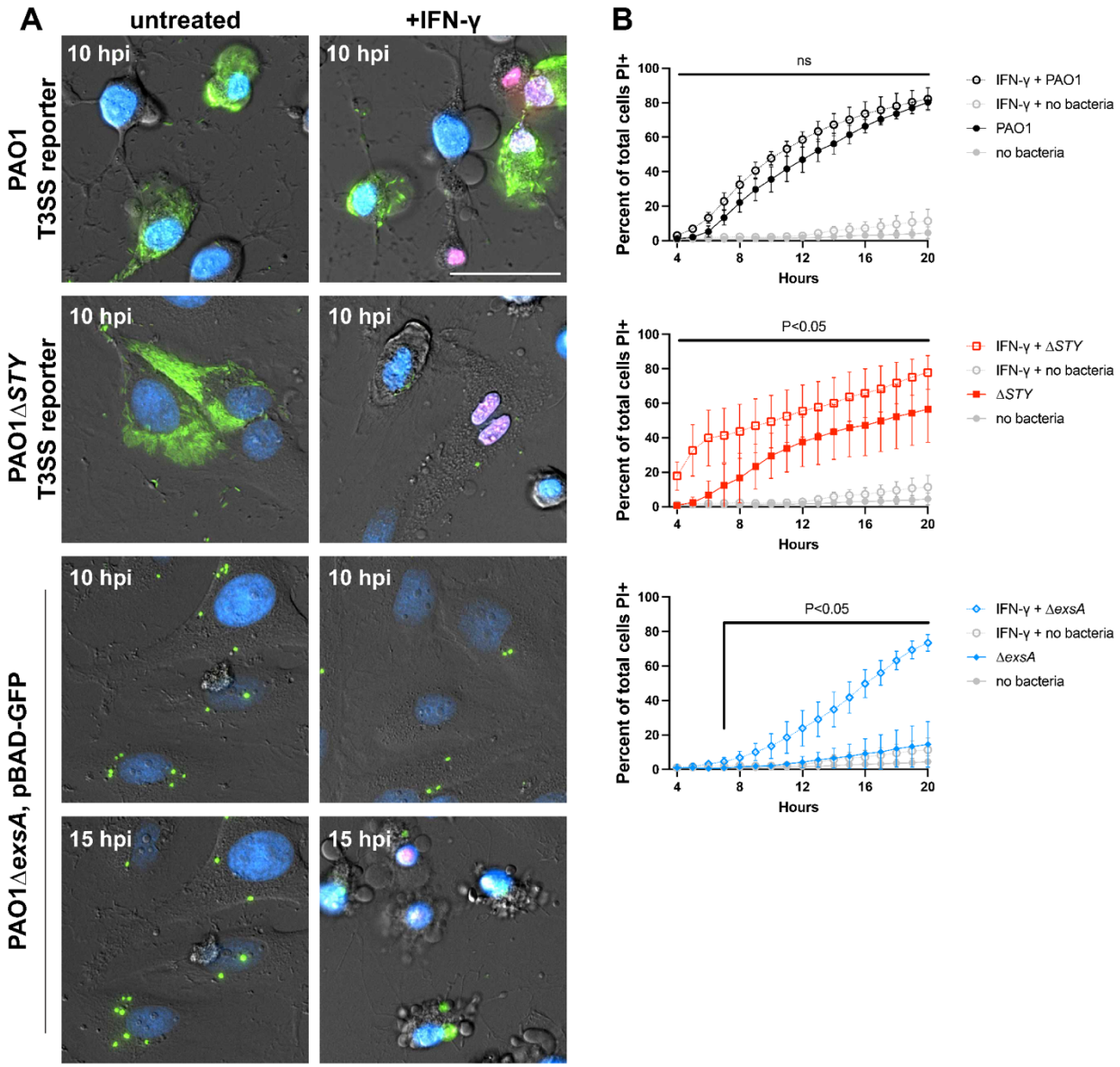

Figure 6. IFN-γ-stimulated HeLa cells are not permissive for PAO1Δ*exoSTY* intracellular replication nor PAO1Δ*exsA* intracellular persistence. (A) HeLa cells were treated with 50 ng/ml IFN-γ for 16 hours prior to infection with wt PAO1, PAO1Δ*exoSTY* (each using the T3SS-GFP reporter) or PAO1Δ*exsA* (pBAD-GFP induced) at an MOI of 10. Nuclei were labeled with Hoechst and propidium iodide. Extracellular bacteria were eliminated with amikacin at 3 hours post infection, and imaged hourly from 4 to 20 hours post infection. Select time frames are shown at either 10 or 15 hours post infection. Scale bar = 50 µm. Full-field time lapses are available as **Supplemental Movie 4**. **(B)** The rate of cell death was determined using host cell nuclear stains. All panels are from the same experiment with only indicated bacterial strain shown. Error bars show SD from three replicates. Multiple column t-tests were performed comparing IFN-γ-treated cells to untreated.

Supplemental Figure 1

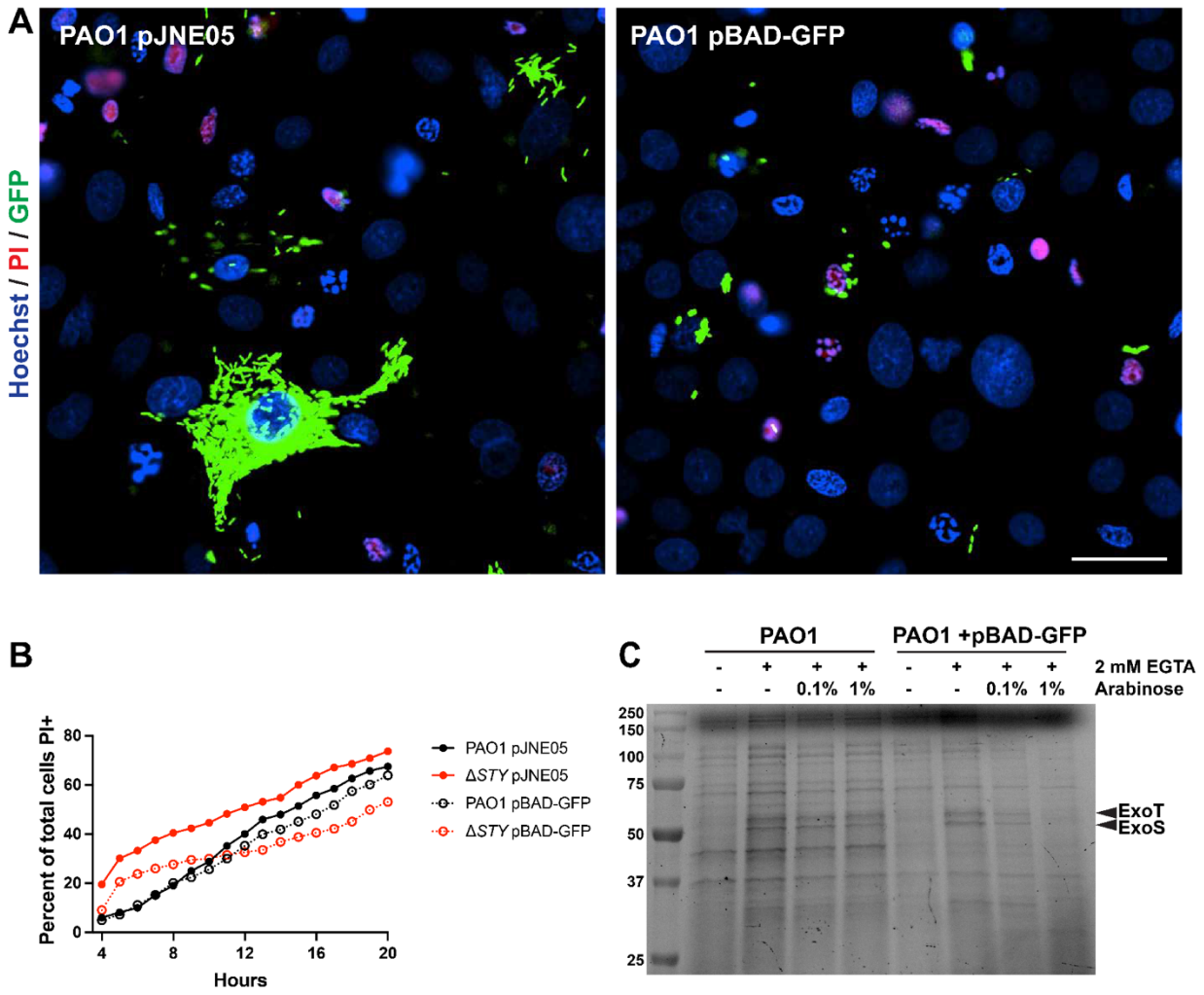

Supplemental Figure 1. GFP expression from plasmid pBAD-GFP suppresses the T3SS. (A) wt PAO1 was transformed with the T3SS reporter plasmid pJNE05, or the GFP inducible plasmid pBAD-GFP and imaged hourly in time lapse. Example fields are shown in which bacteria expressing GFP under the T3SS reporter exhibit intracellular spread and replication, whereas those with inducible GFP show only limited intracellular replication. (B) The cell death rates of wt PAO1 or PAO1Δ*exoSTY* expressing GFP by either plasmid were measured, showing a trend of reduced cell killing rates for PAO1Δ*exoSTY* when GFP expression is induced. (C) wt PAO1 with indicated plasmid was grown for 5 hours in LB media with EGTA to induce the T3SS, and arabinose to induce GFP. Supernatant proteins were concentrated by TCA precipitation, and the bands constituting ExoS and ExoT are indicated.

Supplemental Figure 2

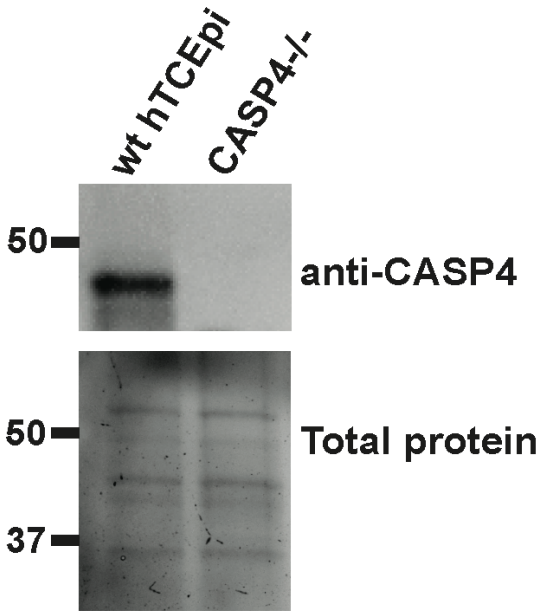

Supplemental Figure 2. Confirmation of caspase-4 deletion. Lysates from wt hTCEpi cells or caspase-4 candidate knockout cells were collected in RIPA buffer and clarified. Total protein was visualized using Bio-Rad stain free gels prior to transfer. Blot was probed with anti-caspase-4 antibody.

Supplemental Figure 3

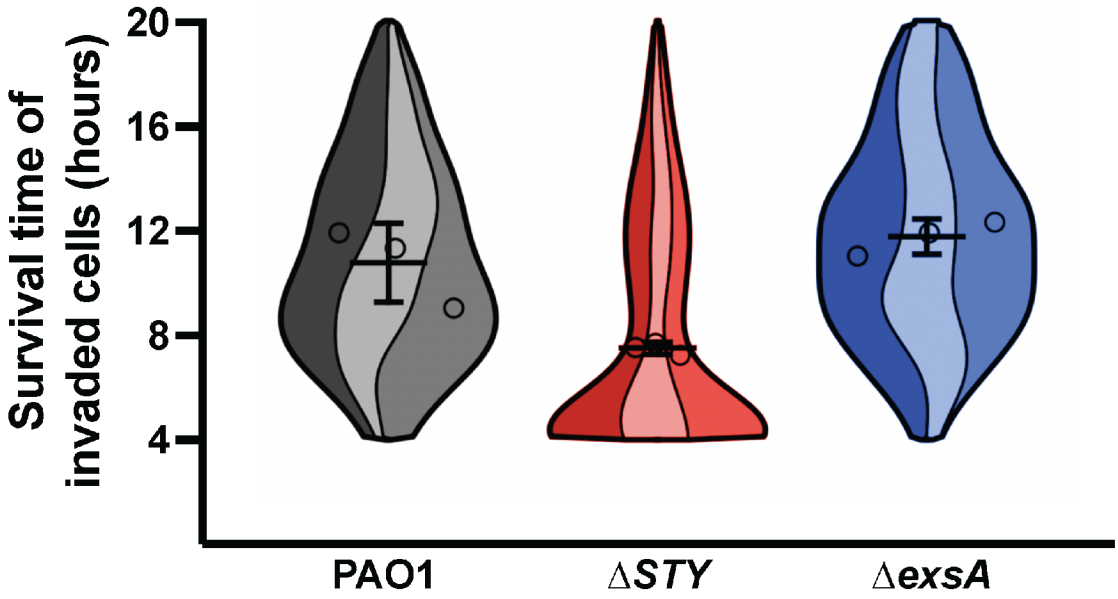

Supplemental Figure 3. Control monoclonal cells for CRISPR-Cas9 mutagenesis. A control cell line was generated using non-targeting guide RNA, and monoclonal line generated. Cells were infected with wt PAO1, PAO1Δ*exoSTY* (each using the T3SS-GFP reporter) or PAO1Δ*exsA* (pBAD-GFP induced) at an MOI of 10. Nuclei were labeled with Hoechst and Propidium iodide. Extracellular bacteria were eliminated with amikacin at 3 hours post infection, and imaged hourly from 4 to 20 hours post infection. Images were analyzed with a computational approach to segregate invaded cells and measure survival times in hours. Three replicates were combined into a single super violin plot. Mean survival times with SD error bars are displayed.

Supplemental Figure 4

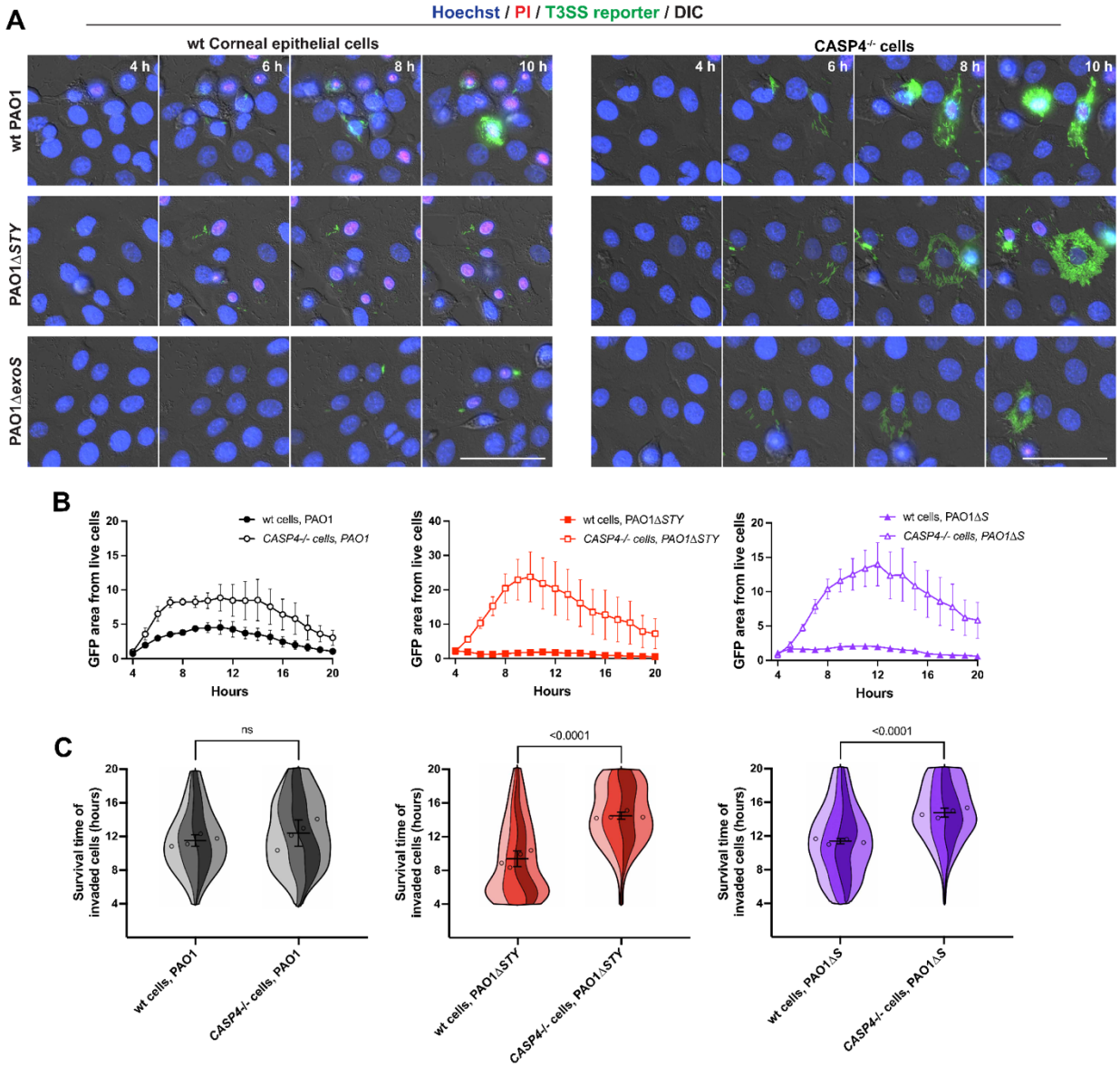

Supplemental Figure 4. Host cell survival time and intracellular replication of single exotoxin deletion of ExoS. (A) Corneal epithelial cells or cells lacking caspase-4 were infected with wt PAO1, PAO1Δ*exoSTY*, or PAO1Δ*exoS* (each visualized by T3SS-GFP reporter) at an MOI of 10. Nuclei were labeled with Hoechst and propidium iodide. Extracellular bacteria were eliminated with amikacin at 3 hours post infection, and imaged hourly from 4 to 20 hours post infection. Images from 4-10 hours are shown. Scale bar = 50 µm. (B) GFP area was summed within the boundaries of live cells and normalized to PAO1 (wt) at 4 hours post infection. (C) Cells from indicated infections were analyzed with a computational approach to segregate only invaded cells and measure survival times in hours. Mean survival times with SD error bars are displayed, and significance determined by Student's t-test.